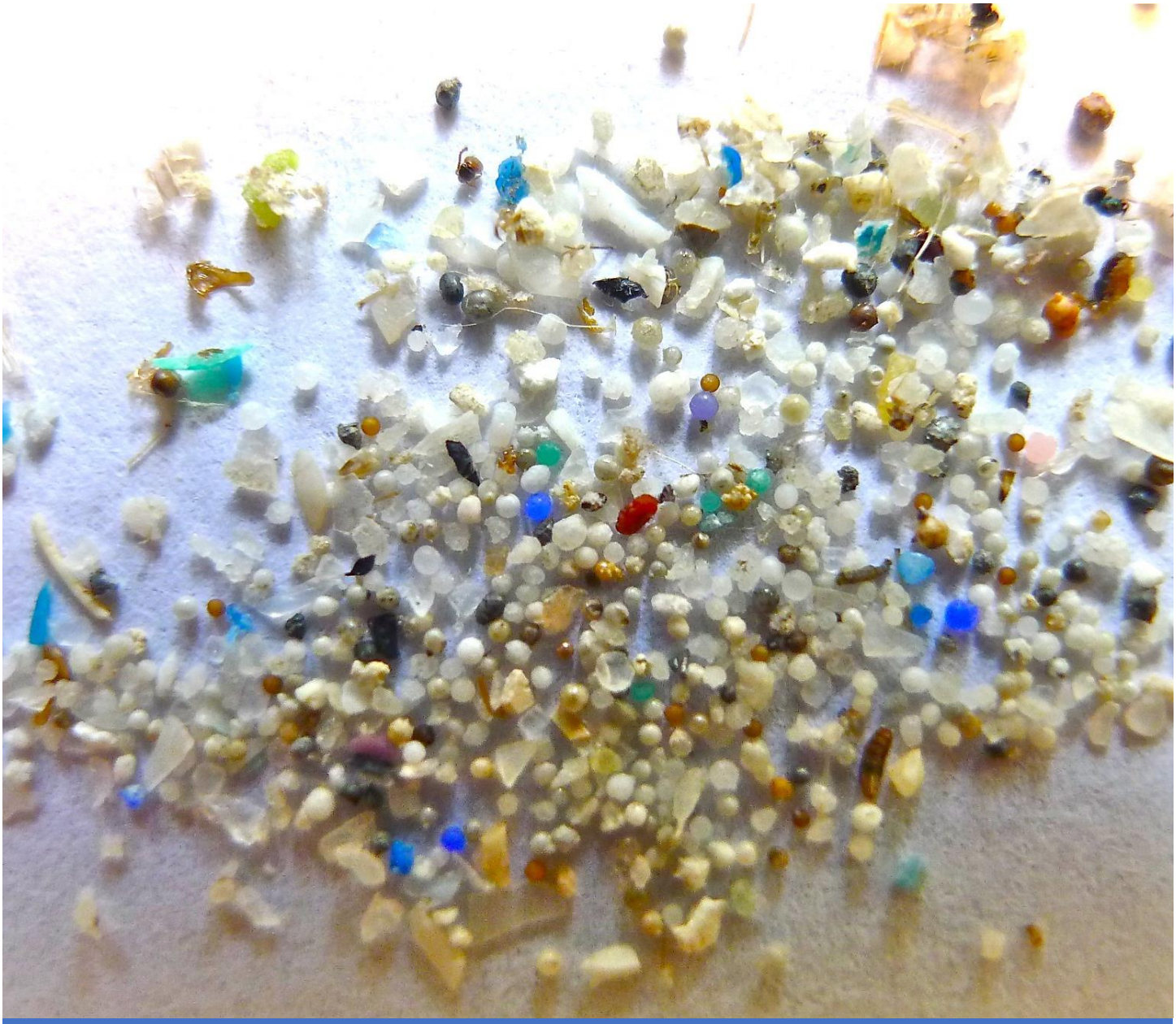

Exploring the Effects of Sample Preparation on Microplastics: Assessing Chemical and Physical Changes and Recovery Rates

Matea Čulina

June 2023

Aalborg University

Aalborg University
Department of the Built Environment
Thomas Manns Vej 23
9220 Aalborg East

Exploring the Effects of Sample Preparation on Microplastics: Assessing Chemical and Physical Changes and Recovery Rates

Master's Thesis (60 ECTS)

Student name: Matea Čulina
Study no: 20211221
Study program: Environmental Science
Project period: September 2022 - June 2023

Supervisor: Jes Vollertsen
Co - Supervisor: Laura Simon-Sánchez

Acknowledgement

I want to thank to my supervisor, Jes Vollersten for allowing me to conduct my master's thesis at the Department of the Built Environment at Aalborg University, for introducing me to this topic, and for his helpful comments and suggestions throughout my work. I am deeply grateful to my co-supervisor Laura Simon-Sánchez for her significant help and support during my entire thesis journey and for creating a comfortable and positive environment during the laboratory and writing phases, making the experience enjoyable. I would like to thank my lab mates and research team at the department for the cherished time spent together in the lab. My appreciation also goes out to my family and friends for their encouragement and support all throughout my studies.

List of Abbreviations

MP - Microplastic

PE - Polyethylene

HDPE - High-Density Polyethylene

PET - Polyethylene Terephthalate

PP - Polypropylene

PS - Polystyrene

PVC - Polyvinyl Chloride

SDS - Sodium Dodecyl Sulfate

SPT - Sodium Polytungstate

$ZnCl_2$ - Zinc Chloride

NaCl - Sodium Chloride

H_2O_2 - Hydrogen Peroxide

NaOH - Sodium Hydroxide

$FeSO_4$ – Iron (II) Sulfate

FT-IR - Fourier Transform Infrared

ATR - Attenuated Total Reflection

IRE - Internal Reflection Element

HPLC - High-Performance Liquid Chromatography

List of Figures

List of Tables

Contents

1. Introduction

Every year, between 4.8 and 12.7 million metric tons (MMT) of plastic waste enters the ocean from land-based sources, and it is estimated that there are now over 5 trillion plastic particles weighing more than 250,000 tons floating in the world's oceans (Eriksen et al., 2017). Microplastics (MPs), which are small plastic particles less than 5 millimeters in size, have become a growing concern due to their potential impact on the environment. MPs can be ingested by a wide range of organisms in aquatic environments, from plankton to whales, and can accumulate in the food chain. Over 100 marine species have been found with MPs in their stomachs, and it is estimated that more than half of all seabirds and sea turtles have ingested plastic debris (Jambeck et al., 2018). A study by Lusher et al. (2013) showed that 36.5% of fish collected from the English Channel had MPs in their gut, with an average of 1.9 MP particles per fish. The ingestion of MPs can lead to reduced growth, reproduction, and survival of the affected organisms, as well as altered behavior and hormonal effects (Galloway et al., 2017). In addition to these impacts on marine life, MPs have been shown to transport pollutants and toxic chemicals, such as heavy metals and persistent organic pollutants, into the food web, leading to potential health risks for both wildlife and humans (Liu et al., 2019., Rios et al.,2007). The potential impacts of MPs on human health are also a growing concern, with some studies suggesting that they may have endocrine-disrupting effects and could potentially cause reproductive and developmental problems (Wagner et al., 2009, Smith et al.,2018).

Given the potential risks associated with MPs, it is crucial to identify sources of MPs, extract them from environmental matrices, and quantify and qualify them. Researchers are actively working on developing methods to detect and quantify MPs in various environmental compartments, including ocean, sediment, and the atmosphere. By understanding the sources and distribution of MPs, we can develop effective strategies to reduce their environmental impact and protect the health of both animals and humans. In recent years, there has been a growing interest in developing standard methods for the analysis of MPs, including methods for sampling, extraction, identification, and quantification (GESAMP, 2015). Several studies have evaluated different sampling techniques and extraction protocols to optimize MP recovery from environmental samples (Rasmussen et al., 2012, Kirstein et al., 2019, Wang et al.,2023, Hansen et al.,2023). To accurately identify the sources of MPs, researchers are also working on developing techniques to fingerprint the MPs using chemical and physical characteristics, such as polymer type, size, and shape. These techniques include Fourier transform infrared spectroscopy (FTIR) and Raman spectroscopy (Primpke et al., 2020).

As the field of MP research continues to evolve, it is becoming clear that a multidisciplinary approach is necessary to fully understand the sources, impacts, and solutions to MP pollution. This requires collaboration among scientists from a range of fields, including engineering, chemistry, biology, ecology as well as policy.

This thesis aims to contribute to the ongoing research on the development of effective standard methods for MPs by investigating the potential impact of different chemicals commonly used for extracting the MPs particles from the environmental matrix. The main objective was to characterize the potential physical and chemical changes on the properties of MP particles during the sample preparation protocol steps (SDS treatment, density separation, enzymatic treatment, and Fenton treatment). The recovery rate of particles after each protocol step was also evaluated. Additionally, different identification techniques, including µFT-IR imaging and µRaman spectroscopy, were compared to determine which method was best suited for the analysis of the samples. To accomplish this, standardized samples with known numbers of spiked particles were utilized. The spiked particles included five main polymer types: polyethylene (PE), polypropylene (PP), polystyrene (PS), polyvinyl chloride (PVC), and polyethylene terephthalate (PET).

By testing the effects of different chemicals and identification techniques, this research can inform future researchers and contribute to the development of standard methods for the analysis of MPs that can be used to identify sources and quantify the extent of MP pollution in the environment.

2. Theoretical background and information

2.1. Defining Plastics

Plastics are synthetic materials made from polymers, which are long chains of repeating molecules (PlasticsEurope, n.d.). These materials can be molded into a variety of shapes and forms, making them useful in many different applications including packaging, construction, and consumer products. Plastics have several desirable properties, including being lightweight, durable, and resistant to water and chemicals. They can also be manufactured at a relatively low cost, making them a popular choice for consumer products. One of the key concerns with plastics is their persistence in the environment. Plastics can take hundreds of years to break down, and when they do, they often break down into smaller and smaller pieces known as MPs (Andrady, 2017).

2.2. Defining MPs

Microplastics (MPs) are small plastic particles, less than 5 millimeters in size (Hartmann et al., 2019). Their size can range from a 1 µm to 5 millimeters, with smaller particles typically being more abundant in the environment (Van et al., 2018). They can be classified into two main categories depending on their source: primary MPs and secondary MPs (Figure 1).

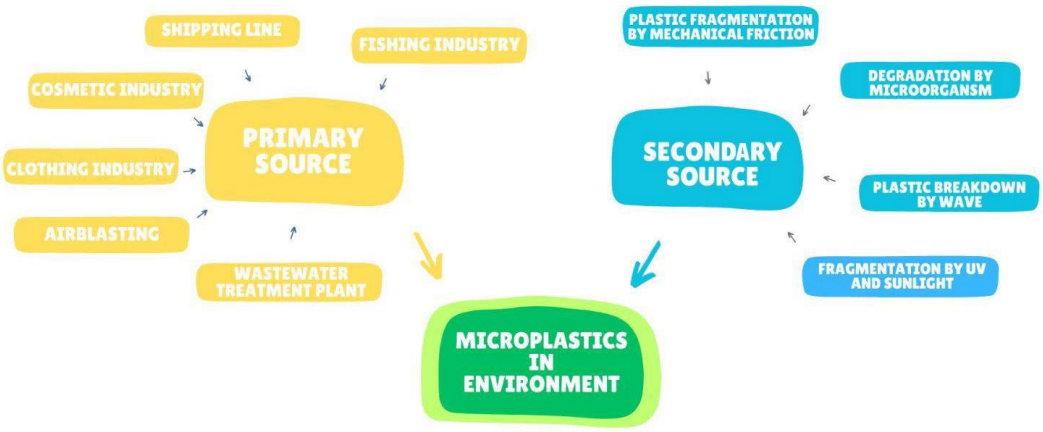

Figure 16. Primary and secondary sources for MPs.

Primary MPs are manufactured and intentionally added to products such as personal care and cosmetic products, industrial abrasives, and plastic pellets used in plastic manufacturing processes. These MPs enter the environment through various pathways, including direct release from product use and manufacturing processes, as well as accidental spills and leaks. Secondary MPs are formed from the degradation of larger plastic items (Cole et al., 2011).

MP debris undergoes degradation through mechanical, chemical, and biological processes in the environment. The rate of degradation is influenced by various polymer characteristics, including their structure and chemical composition. As a result of degradation, MP particles gradually decrease in size, eventually transforming into nanoplastics. (Corcoran, 2022, Guo et al., 2019). In the study by Kalogerakis et al. (2017), there is an experimental investigation focused on polyethylene (PE) films. The research revealed that the degree of weathering was intensified by exposure to sunlight and mechanical stress. Additionally, mechanical weathering of MPs can occur in the water column when particles encounter shear stress forces. Enfrin et al. (2020) conducted an experimental study where PE microbeads from a facial cleanser were released into the water and subjected to shear stress through mechanical stirring, pumping, and ultrasonic irradiation. While mechanical weathering contributes to the fragmentation of MPs, chemical degradation processes such as photooxidation, thermal oxidation, hydrolysis, and differences in salinity and alkalinity can enhance or even initiate the degradation process (Corcoran, 2022). The degradation of MPs can lead to changes in their physical and chemical properties, such as color, surface morphology, crystallinity, particle size, and density (Andrady et al., 2011).

2.2.1. Morphological Characteristics of MPs

MPs are small plastic particles that can take different colors, sizes, and shapes including fragments, pellets, fibers, film, and foams as illustrated in Figure 2. The most common type of MPs found in the environment are fragments, which are small broken-down pieces of larger plastic items. Fragments can come from various sources, such as packaging materials, plastic bottles, and fishing gear. Pellets are another type of MP that can be easily transported by wind and water and are commonly found in marine and freshwater environments. Pellets are small bead-like pieces of plastic that are used as raw materials for plastic manufacturing. Fibers are also a type of MP that can come from synthetic textiles and other materials that shed fibers during usage and washing. Thin, flexible, sheet-like plastics known as film, usually originating from plastic bags, plastic foil, or other packing materials, are also a type of MP. Any kind of plastic with a foamed structure is referred to as foam. This could be, for example, Styrofoam

or other expanded or foamed plastics such as polystyrene (PS), polyethylene (PE), or polyvinyl chloride (PVC). (GESAMP, 2015, Dey et al.,2021).

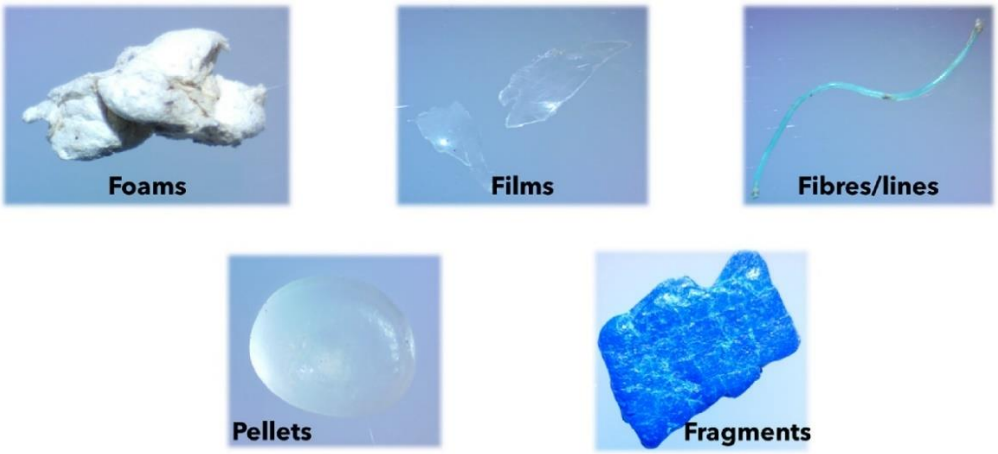

Figure 17. Different shapes of MPs (Jiménez-Skrzypek et al.,2021).

2.2.2. Chemical Characterization of MPs

Apart from different physical properties, MP particles also differ in their chemical composition. MPs are synthetic materials made from polymers, which are large molecules made up of repeating subunits called monomers. The structure of a polymer depends on the type of monomers used and the way they are linked together. The most common polymers found in the environment are polyethylene (PE), polypropylene (PP), polyvinyl chloride (PVC), polystyrene (PS), and polyethylene terephthalate (PET) (Andrady, 2017). They all belong to the group of thermoplastics which are a type of polymers that can be easily melted and molded into various shapes when heated. Unlike thermosetting plastics, which undergo a chemical change during heating and cannot be reshaped once they are set. Thermoplastics can be melted multiple times without undergoing any chemical change, making them suitable for recycling. (Andrady, 2017).

Polyethylene (PE) is a type of polymer composed of ethylene monomer units that are arranged linearly. Depending on the manufacturing process, PE can have different levels of branching and crystallinity. Its low cost and long durability make it a popular choice for packaging and disposable products. Polyethylene terephthalate (PET) is another type of polymer made up of repeating terephthalic acid and ethylene glycol monomer units. It has a highly crystalline structure, which gives it strength and clarity. PET is commonly used in beverage bottles and

food packaging due to its recyclability and other desirable properties. Polystyrene (PS) is made up of repeating styrene monomer units and can be either amorphous or crystalline. PS is used in packaging and insulation materials because of its great insulating properties and affordability. Polypropylene (PP) is a linear polymer made up of repeating propylene monomer units. Depending on the manufacturing process, PP can have different levels of crystallinity. It is often used in packaging, automotive parts, and medical devices due to its chemical resistance and low density. Polyvinyl chloride (PVC) is a linear polymer composed of repeating vinyl chloride monomer units. Like PP, it can have varying levels of crystallinity depending on the production process. Because of its versatility and durability, PVC is commonly used in construction materials, medical devices, and consumer products (PlasticsEurope, n.d.).

Table 4. Table showing common polymers, their chemical structures, and typical applications

Polymer	Chemical Structure	Applications
Polyethylene (PE)	$(C_2H_4)_n$	Packaging, disposable products
Polyethylene terephthalate (PET)	$(C_{10}H_8O_4C_2H_4)_n$	Beverage bottles, food packaging
Polystyrene (PS)	$(C_8H_8)_n$	Packaging, insulation materials
Polypropylene (PP)	$(C_3H_6)_n$	Packaging, automotive parts, medical devices
Polyvinyl chloride (PVC)	$(C_2H_3Cl)_n$	Construction materials, medical devices, consumer products

The durability and resistance of these polymers to degradation can lead to their persistence in the environment and pose a threat to ecosystems. Moreover, their chemical properties can make them prone to leaching toxic additives and interfering with biological processes, causing long-term ecological damage.

2.3. From MPs in the Environment to MPs Identification

As the negative impact of MPs on the environment and human health continues to be a growing concern, research efforts aimed at discovering their sources and reliably identifying and quantifying these pollutants are gaining significant attention. Recognizing the sources and characterizing MPs is essential for implementing effective measures to reduce their release into the environment and mitigate the potential hazard they represent. To quantify MP

particles, it is essential to undergo several steps. The first of which is the sampling, which can be conducted in a variety of environmental matrices such as marine waters or freshwater systems, wastewater, soil, and sediment.

2.3.1. Sampling

Proper sampling practices are crucial for collecting representative environmental samples and minimizing contamination. In the study of Aineli et al., (2021) several approaches for sampling MPs from the environment are described. The first method is selective sampling, which involves collecting directly the plastic items. This method is limited to occasions where the plastic particles are visible to the naked eye and are not suitable for MPs smaller than 4 mm. Another approach is bulk sampling, where a volume of the environmental matrix is collected to later extract the MP in the laboratory. This method is commonly used for benthic sediments and soil matrices. Alternatively, there is the volume-reduced sampling technique, which is commonly used to target the water compartment. Surface water samples are commonly collected using Manta tows, Neuston, and Plankton nets with mesh sizes varying from 333 µm to 25 µm (Kye et al.,2023). One more technique for sampling marine waters is using a pump or centrifuge, although its volume-sampling capacity generally is lower than the one of nets. However, it is suitable for sampling small MPs that may be underestimated from the nets sampling approach (Simon-Sánchez et al.,2022). Sampling for MPs using large-volume pumps has been largely applied to target these pollutants in wastewater treatment plants. The pump usually consists of a filtering device made of metal materials like stainless steel or aluminum, and a glass bottle for storage. (Aineli et al.,2021). For sampling MPs in sediments and soil, the grab sampling method is commonly proposed as it can collect small MPs. Besides, metal tools such as spoons, Van-Veen grab samplers, and metal corers can be used. Last, but not least are the procedures to minimize potential contamination during sampling. It is common practice to use containers made of glass, stainless steel, or aluminum for the collection, storage, and transportation of MP samples, rather than using plastic bottles or containers (Lee et al.,2023).

2.3.2. Sample Treatment

To optimize the recovery and detection of MPs, various sample preparation techniques are available, each suited to specific sample types and research goals. The choice of sample

preparation method depends on the type of sample being analyzed and the specific research questions being addressed.

One of the first steps in sample preparation for MP analysis is pre-oxidation, which involves oxidizing the sample with hydrogen peroxide (H_2O_2) to remove organic material and increase the contrast between the MP particles and the sample matrix. This procedure is usually used for sediment and wastewater samples (Gatidou et al. 2019, Kye et al.,2023). Another method for sample preparation is size fractionation, which involves separating particles based on their size. This is typically done using sieves or filters of different mesh sizes. The procedure can be used to process soil and sediment samples (Carr et al., 2016). To separate MP particles from other organic and inorganic materials present in environmental samples, density separation is applied. This can be done using a heavy liquid such as sodium chloride (NaCl) or zinc chloride ($ZnCl_2$) (Nabi et al.,2022). These chemicals are commonly used in MP research because they can separate MP particles that are lighter than heavy liquids used, allowing denser particles such as sediment grains to sink. Most studies reported using NaCl as a density separation solution due to its low price, high solubility, and low toxicity, however, its density of 1.0-1.2 g/cm^3 limits the recovery of high-density MPs (Kye et al.,2023). While $ZnCl_2$ can reach a density of 1.7 g/cm^3, it is corrosive and toxic. To overcome this issue, some studies are alternatively using sodium poly tungstate (SPT) (Molazadeh et al.,2023, Lenz et al.,2023) because of its high density (1.4–1.6 g/cm^3) and low toxicity compared to $ZnCl_2$, but it is significantly pricey. This preparation step is usually followed by SDS treatment. Sodium dodecyl sulfate (SDS) is a detergent that can dissolve lipids and proteins. The addition of SDS to samples can also help to disaggregate MPs that may be clumped together or embedded in organic matter (Kirstein et al.,2019, Ainali et al.,2021). Enzyme treatment is another step used to remove organic matter from MP particles. This method involves treating the sample with enzymes such as proteinase K or cellulase, which can break down proteins and carbohydrates (Löder et al.,2017). Additionally, one method also used to break down organic matter in the sample is Fenton oxidation. This procedure involves using a solution of hydrogen peroxide (30% H_2O_2) and ferrous sulfate ($FeSO_4$) to generate hydroxyl radicals (•OH) in the sample solution, which are highly reactive and can oxidize organic compounds (Lavoy et al.,2021).

2.3.3. Methods of Detection

Typically, the detection of MPs can be divided into two stages: physical identification based on characteristics such as color, shape and size, and chemical identification based on their

polymer composition (Dey et al.,2021). Two widely used methods for chemically identifying MPs are Fourier Transform Infrared Spectroscopy (FT-IR) and Raman Spectroscopy.

2.3.3.1. Fourier Transform Infrared (FT-IR) Spectroscopy

Fourier Transform Infrared (FT-IR) Spectroscopy is an analytical technique that provides information about the chemical composition of a sample. It is a non-destructive and rapid method that allows for the identification and quantification of chemical compounds in a variety of samples. FT-IR spectroscopy measures the infrared radiation transmitted by a sample as a function of wavelength, producing a spectral fingerprint that can be used for identification (Khan et al.,2018). Transmission FT-IR spectroscopy involves passing the infrared beam through the sample, which causes the molecules to vibrate and absorb certain wavelengths of light. The intensity of the transmitted light is measured, and the spectrum of the sample is obtained (Khan et al.,2018). It involves the use of a specialized instrument called an FT-IR spectrometer. The main components of an FT-IR spectrometer are the source, interferometer, sample compartment, and detector (Baker et al.,2014). The source produces infrared radiation that is directed into the interferometer, where it is split into two beams that travel different paths. One beam passes through the sample, while the other beam passes through a reference material. The two beams are then recombined, and the resulting interference pattern is measured by the detector (Harvey, 2022).

Another way that FT-IR spectroscopy can be performed is using reflection as shown in Figure 3.

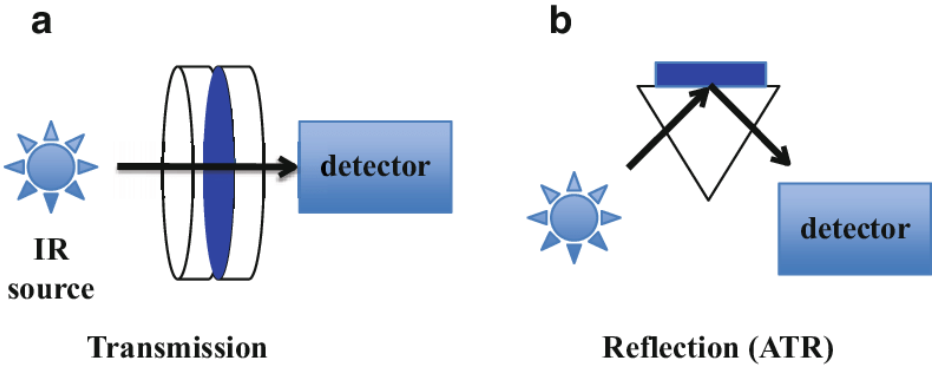

Figure 18. FTIR sampling methods. (a) Transmission. (b) Reflection Source: https://www.researchgate.net/figure/FTIR-sampling-methods-a-Transmission-b-Reflection_fig1_338968819.

The principle of total internal reflection is used in Attenuated Total Reflectance Spectrometry. The beam propagates through the sample, is absorbed by the sample, and the intensity of the radiation is reduced. The degree of absorption is dependent on the chemical composition of

the sample, and the wavelengths of the absorbed radiation are characteristic of the sample's functional groups (Harvey,2022). The ATR accessory consists of an internal reflection element (IRE) that is made of a material with a high refractive index, such as diamond or zinc selenide. The IRE is in contact with the sample, and the beam of infrared radiation is reflected multiple times between the IRE and the sample surface, resulting in a high degree of interaction between the radiation and the sample. The reflected beam is then collected and analyzed to produce an ATR spectrum (Glassford et al.,2013).

The study of Primpke et al. (2020) explains some of the limitations of FT-IR spectroscopy when it comes to analyzing MP particles. One of the main limitations is the inability to identify very small particles (less than 10 µm) using FT-IR spectroscopy due to their low signal intensity. Another limitation is the potential interference of the sample matrix in the spectral analysis, which can result in false positives or negatives. The presence of other substances in the sample, such as minerals, can interfere with the FT-IR spectra and make it difficult to identify MPs. The lack of standardization in sample preparation and analysis can lead to variability in results between different laboratories and researchers.

2.3.3.2. Raman Spectroscopy

Raman Spectroscopy is a non-destructive analytical technique that provides information about the vibrational modes of molecules in a sample (Harvey,2022). It is based on the Raman effect, which involves the scattering of light by molecules in the sample, leading to a shift in the wavelength of the scattered light. When a photon of light interacts with a molecule, it can be scattered in several ways as shown in Figure 4. In elastic scattering (Rayleigh scattering), the scattered photon has the same frequency and wavelength as the incident photon. In inelastic scattering (Raman scattering), the scattered photon has a different frequency and wavelength, resulting in a Raman shift. (Harvey,2022). The Raman shift provides information about the vibrational modes of the molecule, which are related to its chemical structure and composition. (Carey,1999). The basic components of a Raman spectrometer include a laser source, a monochromator, a sample compartment, and a detector. The laser source provides the monochromatic light, which is then focused on the sample. The scattered light is then collected by the monochromator and directed to the detector. The Raman spectrum is obtained by plotting the intensity of the scattered light as a function of the Raman shift (Bumbrah et al.,2016).

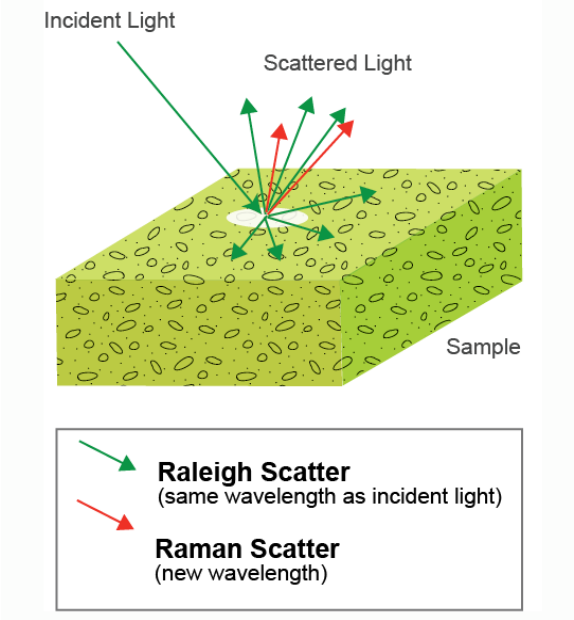

Figure 19. Principle of Raman spectroscopy found on: https://www.princetoninstruments.com/learn/raman.

Three approaches can be used for MP analysis with Raman spectroscopy: manual measurement of single particles, automated particle identification with the "Particle Finding" algorithm, or point-by-point mapping with "Imaging Mode" (Primpke et al.,2020). For automated particle identification, an appropriate filter material must be used to ensure reliable and reproducible analysis. Image analysis software is used to detect and measure particles automatically (Primpke et al.,2020, Anger et al.,2018).

While Raman spectroscopy is a highly effective analytical technique, it is not without its limitations. One of the primary challenges associated with Raman spectroscopy is fluorescence interference from certain samples, which can overpower the Raman signal and potentially compromise the accuracy of spectral analysis (Primpke et al.,2020). Moreover, Raman spectroscopy can be impacted by sample heating or laser-induced damage, which may modify the sample and interfere with the spectral analysis (Primpke et al., 2020). Therefore, it is essential to carefully consider these potential limitations when conducting Raman spectroscopy analyses to ensure accurate and reliable results.

3. Materials and Methods

3.1. Large MPs (0.5 - 3 mm)

To investigate larger MP particles, ten grinded MP particles of five different polymer types were used, making a total of 50 MP particles. The types of polymers used include PVC (Polyvinylchloride), PS (Polystyrene), PP (Polypropylene), PET (Polyethylene Terephthalate), and HDPE (High-density polyethylene). Particles were divided into ten different batches labeled with numbers 1 to 10, each batch containing five distinct polymer types placed on ø 47 mm stainless-steel filter and arranged in individual Petri dishes as illustrated in Figure 5.

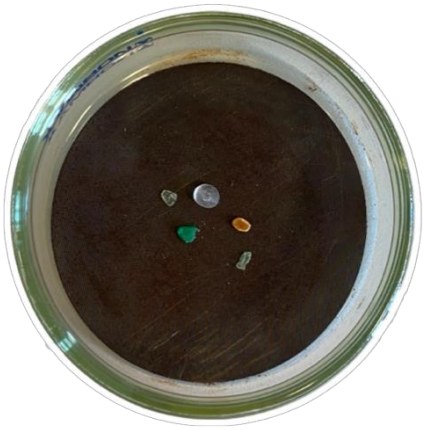

Figure 20. MP particles of five investigated polymers placed on steel filter in Petri dish.

3.1.1. Attenuated Total Reflection (ATR) Spectroscopy and Microscopic Imaging

Before starting with the experimental protocol, initial particle properties were examined. Due to the larger size of the particles, their spectroscopic characteristics were analyzed using Attenuated Total Reflection (ATR) spectroscopy, while their morphology and structure were assessed through microscopic imaging. This analyzing technique was used before and after each protocol step to ensure a comprehensive understanding of any potential modifications in the particle properties. As the ATR analysis technique has the potential to alter the shape of the particles, it was employed before capturing microscope images. Achieving good contact between the sample and the internal reflection element (IRE) of the attenuated total reflection (ATR) objective is necessary for accurate analysis. However, the small contact area increases the risk of sample damage (Morgado et al., 2021).

The ATR analysis was performed using The Agilent Cary 630 FTIR spectrometer equipped with a single reflection diamond ATR sampling module (Figure 6). The scan was collected at 4 cm^{-1} spectral resolution with 64 scans and a spectral range between 560 and 4000 cm^{-1}. The same settings apply to background and sample scans. Each MP particle was scanned individually. The data acquisition process was conducted using the Agilent MicroLab software. Before starting the sample scan, the background was collected by scanning the empty diamond interface. The particle was then placed on the crystal and pressed down using a swivel press to ensure optimal contact between the particle and the crystal. During the sample placement, the live view assessment of the particle-to-diamond contact was monitored. If the contact was low, the sample was repositioned and the clamp was adjusted accordingly. Following that, the scan was performed and the software automatically compared the measured particle spectra to the reference spectra in the library to identify the particle. Once the measurement was completed, the particle was recollected, and the crystal was cleaned with a 50% ethanol solution.

Figure 21. The Agilent Cary 630 FTIR spectrometer equipped with a single reflection diamond ATR sampling module and Agilent MicroLab software.

The microscopic images of particles were acquired using the Zeiss SteREO Discovery.V8 microscope equipped with a Zeiss Axiocam 105 color camera is shown in Figure 7. Particles were individually placed on a glass microscope slide and observed under the microscope. Images were captured at different magnifications, depending on the size of the particle being observed.

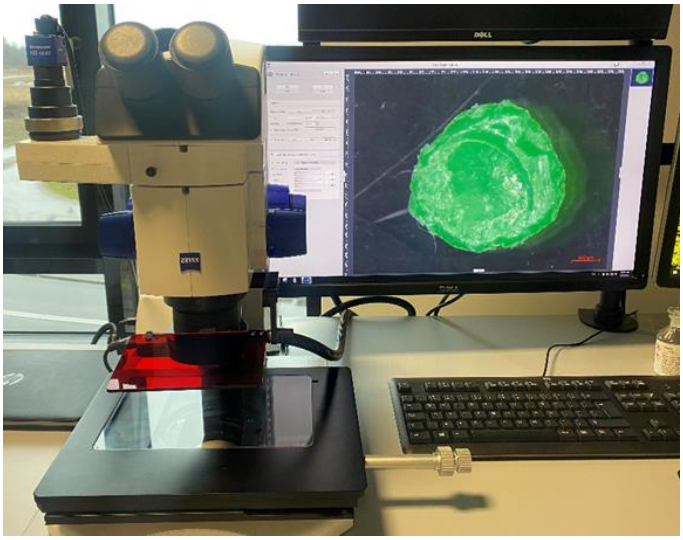

Figure 22. Zeiss SteREO Discovery.V8 microscope equipped with a Zeiss Axiocam 105 color camera and Zen Microscopic Software.

3.1.2. Sample Preparation Protocol

Given that the objective of the study is to assess the impact of certain chemicals (Figure 8.) commonly used in the sample preparation process (references to studies conducted in Aalborg), only the protocol steps involving the use of these chemicals were examined.

Figure 23. Chemicals (from top left to bottom right: SDS, Tris Buffer, Acetate Buffer, H_2O_2, NaOH, $FeSO_4$, SPT, and $ZnCl_2$) used for MP sample preparation protocol.

The procedure (Figure 9.) begins with the placement of each MP batch in a separate 1 L beaker containing 200 mL of 5 % SDS (sodium dodecyl sulfate) solution for soaking. Following this, all ten samples were stirred via a shaker in a water bath for 48 hours. The water temperature was maintained at 50°C, and the shaking was set at 100 rpm. After 48 hours of soaking, the samples were filtered using ø 47 mm steel filters (mesh 10 µm) and rinsed with water to remove any chemical residue from the particles. The particles placed on steel filters were returned to a petri dish, let to dry, and prepared for analysis. The filtration and scanning processes were performed between each protocol step. After scanning, the samples were returned to the same beaker, filled with 250 mL of Tris Buffer solution (pH 8.2) and 500 µL of Protease enzyme. The samples were, again, subjected to shaking in a water bath for 48 hours. The same procedure was repeated for the next step, which involved treating the samples with 250 mL of Acetate Buffer solution (pH 4.8), as well as adding 500 µL of Cellulase enzyme and 500 µL of Viscozyme enzyme. The following protocol step involves Fenton oxidation. To initiate the Fenton oxidation reaction, 200 mL of water, 145 mL of 50% H_2O_2 (hydrogen peroxide), 65 mL of 0.1 M NaOH (sodium hydroxide), and 62 mL of 0.1 M $FeSO_4$ (ferrous sulfate) were added to the beaker containing the particles. During the reaction, monitoring and maintaining a temperature range of 20-30°C using an ice water bath and thermometers was essential. The final stage of the sample preparation protocol, where chemicals are applied, is the density separation of the particles. Since the primary objective is to examine the impact of chemicals on particle properties, the use of separation funnels was unnecessary. Rather, the particles were soaked directly in beakers. The most commonly used chemicals for density separation include SPT (sodium poly tungstate) and $ZnCl_2$ (zinc chloride) (ρ=1.7-1.8 g cm^{-3}). To this end, five samples were soaked in 50 mL of SPT, while the remaining five samples were immersed in 50 mL of $ZnCl_2$. After 24 hours, the particles were rinsed thoroughly with water, dried, and prepared for final scanning.

To reduce contamination from equipment used during the sample preparation protocol, the lab tools were flushed three times with pre-filtered (0.7 µm) water before use. Steel filters used for filtration were muffled at 500°C and beakers with samples were covered with aluminum foil to minimize airborne contamination.

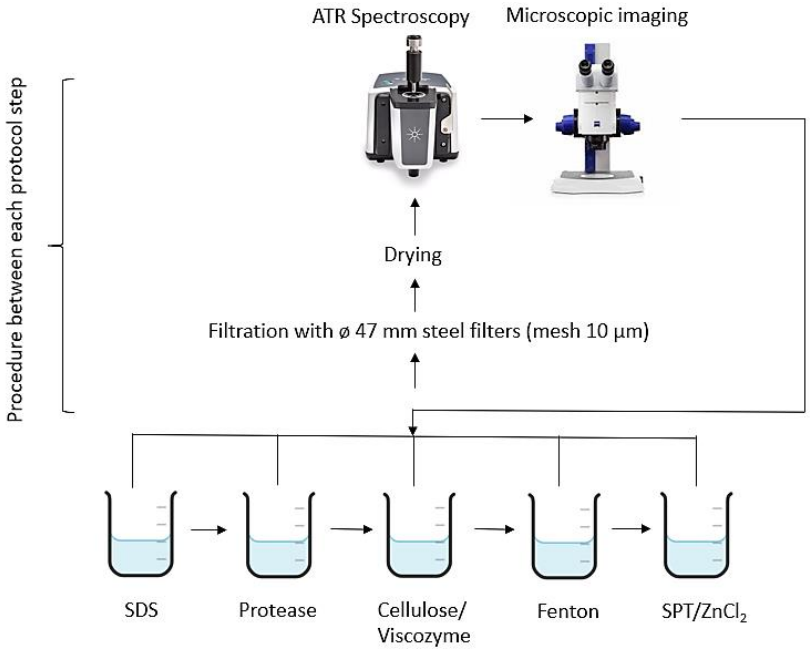

Figure 24. Diagram showing sample preparation steps in treatment of large MP particles.

3.2. Small MPs (3-200µm)

A set of grinded MP particles with sizes ranging between 3 and 200 µm was employed to investigate the smaller MP particles. The particles consist of PVC (20-40 µm), HDPE (80-150 µm), PP (3-100µm), PS (100-200µm), and PET (80-150 µm). These particles were mixed in 10 mL glass headspace vials with a 50% ethanol solution. To create a solution that includes all types of polymers, a measured aliquot of 1 mL was taken from each individual solution and combined in a new vial labeled as "mixed MP" as illustrated in Figure 10.

Figure 25. Small MP particles (PS, PVC, PP, HDPE, and PET) and a mixed solution of these.

3.2.1. Sample Deposition, Fourier-Transform Infrared (FT-IR) and Raman Imaging

To characterize the small MPs with Raman imaging and Fourier-transform infrared (FT-IR) analysis, an aliquot (100 µL) of the mixed MP solution was carefully deposited onto a ø 13 mm silicone membrane with a pore size of 5 µm (Figure 11.) using a stainless-steel filtration funnel (EMD Millipore Corporation, USA), as illustrated in Figure 11. In total, eight silicone membranes with deposited MP particles were prepared. Silicone membranes were selected as the substrate for Raman and µFT-IR analysis due to their compatibility with both techniques.

Figure 26. Silicone membranes (on left: empty membrane, on right: with deposited MP particles) and funnel assessed for depositing particles.

Of the total number of membranes used in the experiment, five membranes (labeled with numbers 1, 3, 5, 7, and 8) were used to examine the recovery rate of the particles after each protocol step together with the distribution of the particles. The remaining three membranes (numbers 2, 4, and 6) were used to compare the efficacy of two different sampling techniques – µFT-IR imaging and Raman imaging.

The µFT-IR measurements were performed using an Agilent 620 FTIR microscope equipped with a 128 ×128 pixel MCT-FPA detector (Mercury Cadmium Telluride–Focal Plane Array) coupled with a Cary 670 FTIR spectrometer (Agilent Technologies, Santa Clara, CA, USA) (Figure 12.) The analysis was performed using a 15-Cassegrain (visible IR) objective-condenser system operated in transmission mode. Firstly, a background scan of a new silicone membrane was taken at 8 cm^{-1} spectral resolution, using 120 co-added scans in the spectral range of 3750–850 cm^{-1}. To obtain an optical image of the sample, single field-of-view images were captured with a 15× objective and then pieced together to cover an area measuring about 14 mm x 14 mm. After capturing the image, an area of 15x15 tiles was scanned with 30 co-added scans and with the same settings as for the background scan.

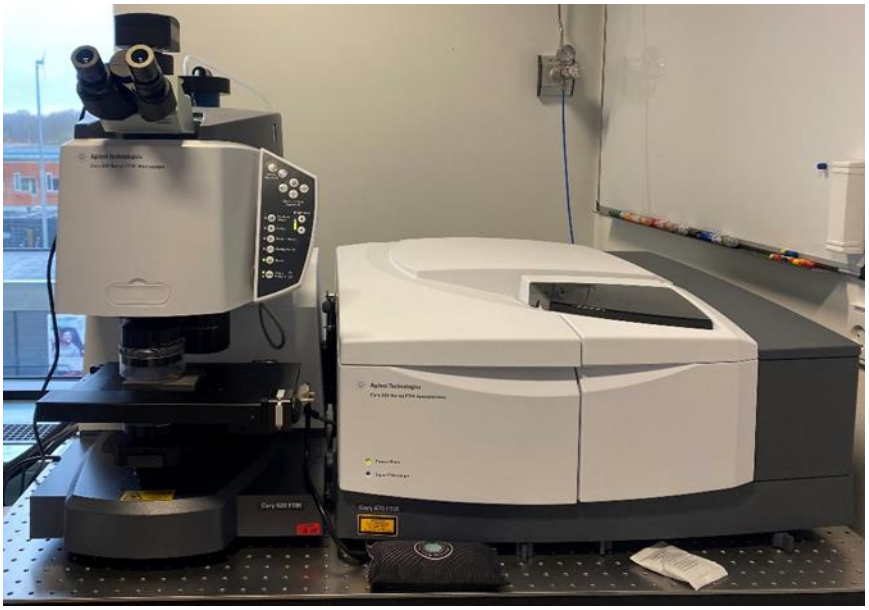

Figure 27. Cary 620 µFT-IR microscope together with a Cary 670 FT-IR spectroscope manufactured by Agilent Technologies.

The Raman spectra of MP particles were collected using a Horiba XploRA PLUS Raman microscope (Figure 13.) equipped with a 750 nm laser excitation source and a 638 nm edge long-pass filter. To perform the analysis, the membrane with the particles was placed on a glass microscope slide and positioned under the objective lens using a motorized stage. The laser was focused onto the particles using a 50x objective lens. The acquisition parameters were set to an integration time of 2 seconds and 4 accumulations. This setup was chosen to maximize the signal-to-noise ratio and obtain high-quality spectra. It should be noted that the instrument was set to scan particles larger than 10 µm. The spectra range was put between 0 and 3500 cm^{-1}. The scanning procedure involved a two-step process. Firstly, a visual image of the sample was captured using the microscope's built-in camera to locate and visualize the particles on the membrane surface. Once the particles of interest were identified, the laser beam was focused on them, and a Raman spectrum was collected at the center of every particle identified (>10 µm). The data was analyzed using LabSpec 6 software, which allowed for real-time monitoring of the acquisition process and visualization of the obtained spectra.

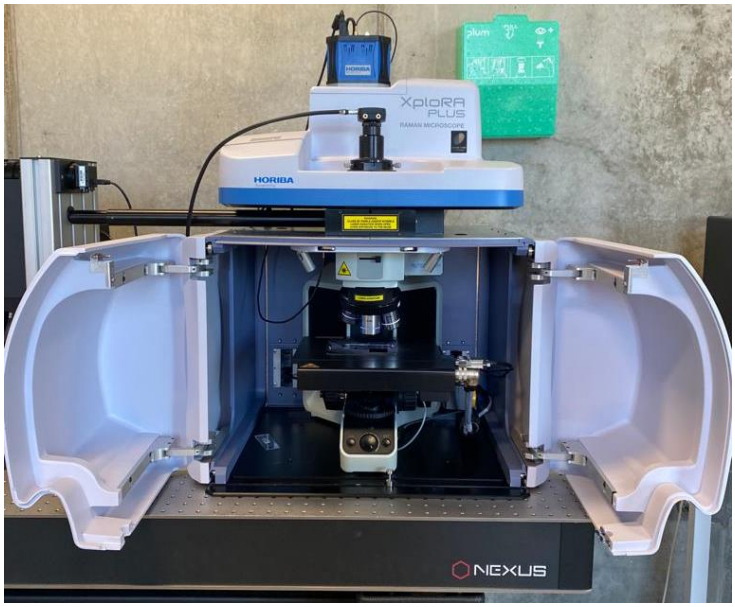

Figure 28. Horiba XploRA PLUS Raman microscope.

Upon analyzing the scan results obtained from Raman and µFT-IR before sample treatment, as well as the appearance of samples after the application of the protocol, it was decided to proceed with only µFT-IR analysis.

3.2.2. Sample Preparation Protocol

To resuspend the MP particles from the silicone membranes, each of the five membranes (numbers 1, 3, 5 ,7, and 8) was individually placed in a 25 mL beaker containing 15 mL of 5 % SDS solution. The beakers were then subjected to sonication in a sonication bath for 3 minutes. After sonication, the membranes were rinsed and returned to their respective stands. The contents from each small beaker were transferred to pre-cleaned 1 L beakers filled with 200 mL of SDS solution. The sample preparation protocol described in Chapter 1.2. was followed, which consists of five steps. However, in this case, the samples were filtered directly through the same silicone membranes used for depositing the particles. After each protocol step, one of the membranes was set aside for µFT-IR scanning, as the goal was to evaluate the impact of each step on the recovery rate and distribution of the particles. (Figure 14.).

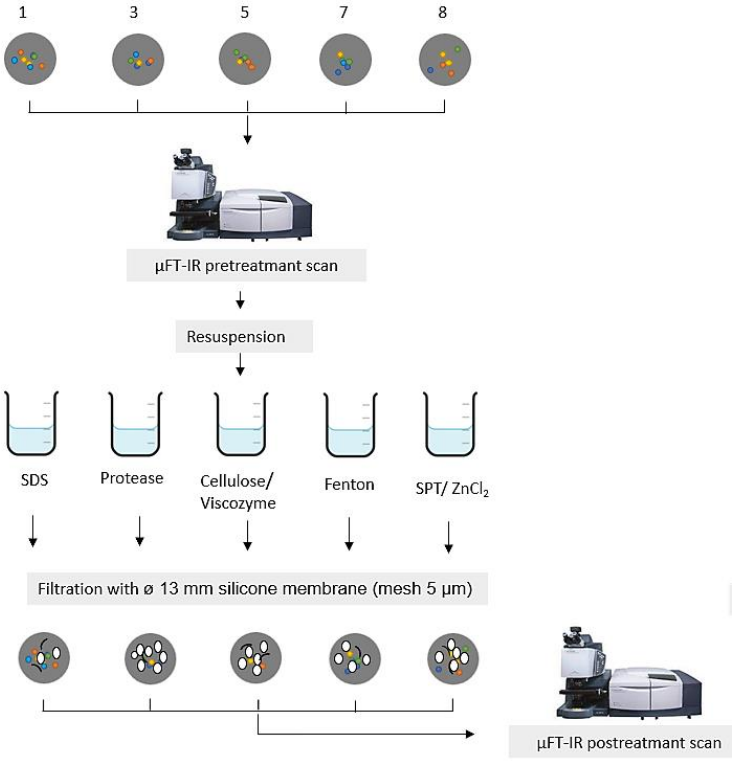

Figure 29. Diagram showing treatment procedure of small MP particles.

Following direct filtration of the samples through a silicone membrane, it was noticed that the membranes were covered with chemical residues, forming a "cake" (Figure 15.) that covered MP particles interfering with the scanning process, particularly after enzymatic treatment. Because of this, the membranes were resuspended in a 50% HPLC ethanol solution and then filtered through ø 47 mm stainless-steel filters with a mesh size of 10 µm in order to rinse the chemical residues. The steel filters were sonicated for 5 minutes to resuspend the particles, and the resulting solution was once again filtered through the silicone membranes.

Figure 30. "Cake" formed as a result of chemical residues after direct filtration of samples (on right: after cellulose and viscozyme treatment, on left: after Fenton oxidation) through silicone membrane.

3.3. Data Processing

3.3.1. siMPle Software

During the research, all data collected from µFT-IR and Raman analysis were processed using siMPle software. SiMPle is an open-source software developed collaboratively by Aalborg University and the Alfred Wegener Institute. It facilitates the automated analysis of extensive mFTIR-Imaging datasets (Rist et al.,2020). The software analyses data sets by calculating the spectral fit between the data and reference spectra using Pearson's correlation for the untreated data, the first derivative, and the second derivative. (Primpke et al.,2020). By reconstructing individual particles based on the FT-IR spectra of the pixels they cover, siMPle generates a false-color map that highlights the identified materials within the sample. Additionally, the software provides assessments related to the morphology and size of the identified particles (Rist et al.,2020, Primpke et al.,2020).

3.3.2. ImageJ Software

The ImageJ software was used to process the captured images of large MP particles after microscopic imaging described in Chapter 3.1.1. to gain information about the size of particles. The captured images underwent pre-processing procedures to optimize the accuracy of the results. The images were transferred into an 8-bit format, and a threshold application was employed to automatically analyze the particles and generate measurements.

3.3.3. SpectraGryph Software

SpectraGryph is a software tool that was used to compare and analyze spectra of large MP particles after their analysis using ATR spectroscopy. The software provided for the characterization of changes in the chemical structure of the particles after each of the sample preparation protocols. The spectra were imported into the software and plotted on a graph, where they could be easily compared and analyzed. SpectraGryph also allowed for the manipulation of the data, including baseline correction and peak fitting. To ensure accurate comparisons, the spectra underwent normalization and baseline correction to eliminate any inherent variations. Normalization was used to scale the intensity of spectral peaks to a standard range or reference point which helps to remove variations in peak intensities. By normalizing the spectra, the relative differences in peak heights can be accurately compared, allowing for a more accurate analysis of the chemical changes in the particles. Baseline

correction was employed to remove background noise that can cause fluctuations in baseline spectra. After normalization and baseline correction, the spectra were saved as CSV text files, which were then used to calculate Pearson correlation coefficients using R Studio software. The Pearson correlation coefficient measures the strength and direction of the linear relationship between two variables. A value close to 1 indicates a strong positive correlation, while a value close to 0 suggests a weak or no correlation between the variables. This statistical approach made it possible to quantify the similarities or differences between spectra, helping in the detection of any significant changes in the chemical structure of the particles.

4. Results and Discussion

4.1. Physical and Chemical Properties of Large MP Particles (0.5 – 3 mm) After Sample Preparation

4.1.1. Morphological Characterization

Microscopic imaging was conducted to visually assess any changes in the shape or color of the MP particles. To illustrate the effects of these changes, one particle from each polymer type was selected as an example and presented in Figure 16. The selected examples are representative of the overall changes observed in all the particles tested.

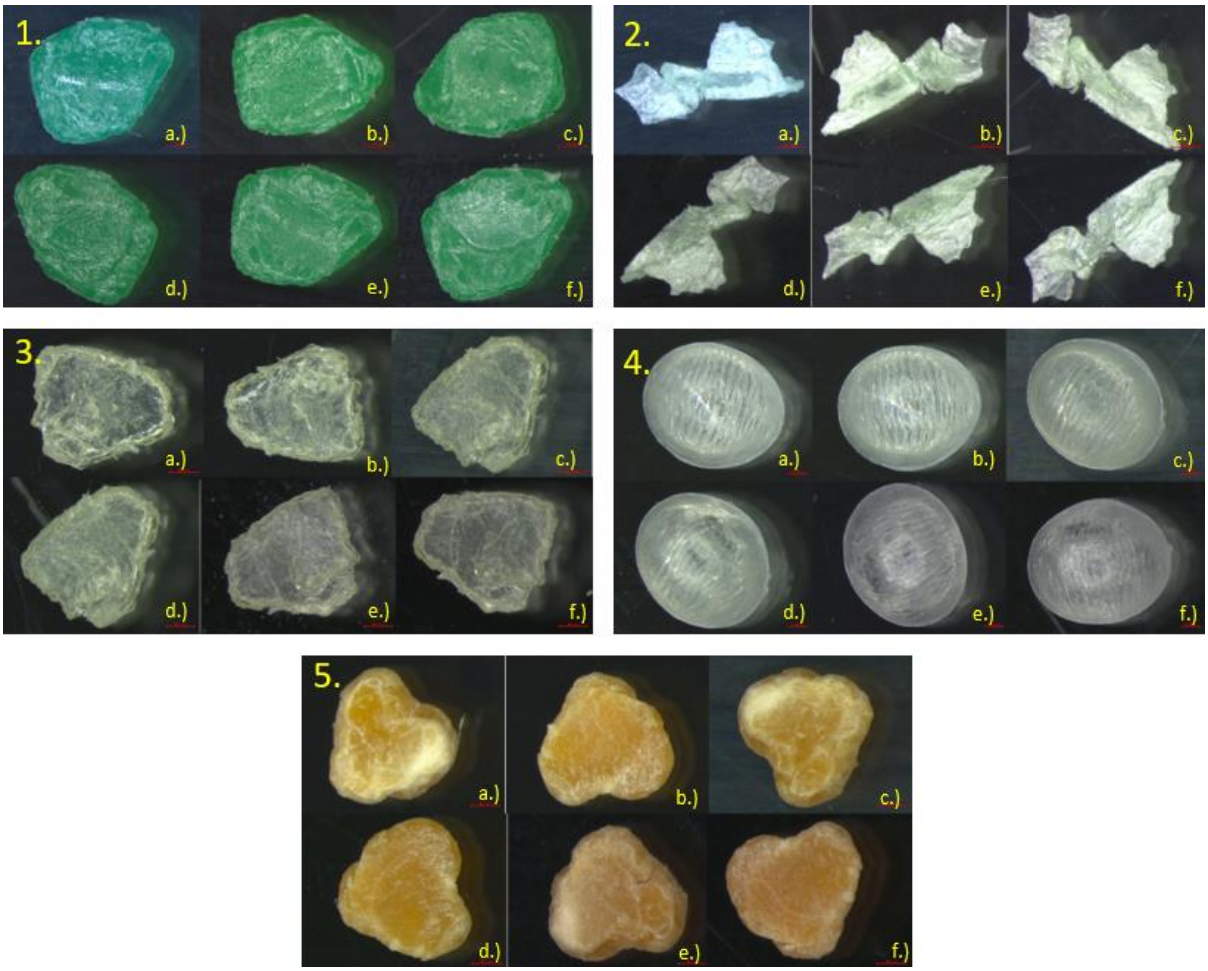

Figure 31. Microscopic images of HDPE (1.), PET (2.), PP (3.), PS (4.), and PVC (5.) particles taken before and after each of the sample preparation treatments. The initial appearance of each particle is shown in image a, while images b through f show the particles after undergoing specific treatments, including SDS (b), protease (c), cellulose and viscozyme (d), Fenton oxidation (e), and density separation (f). Projected areas for particles are: 4.42-4.73 mm^2 (HDPE), 3.79-4.16 mm^2 (PET), 3.92-4.34 mm^2 (PP), 11.47-11.72 mm^2 (PS), 3.81-4.06 mm^2 (PVC).

Upon visual observation of the particles after undergoing the sample preparation procedures, no significant changes were noticed in the shape and color of the particles. Although some particles appeared to have a slightly lighter color, this was determined to be due to different microscopic lighting during image capture rather than the effect of chemicals used during the preparation. Additionally, the particles were not consistently imaged from the same side, which may have contributed to some variations in their appearance. It is worth noting that before the imaging process, the particles underwent ATR spectroscopy, which involved pressing them for analysis. This process may have altered the shape of thinner particles such as PET or PP. Therefore, this visual characterization is considered to be observational and not accurate enough to draw definitive conclusions about the impact of the sample preparation on the particle morphology and appearance. To avoid the problem of the light affecting the color of the particles, before taking the image, there should be standardized lighting conditions ensuring consistent and controlled light during the image capture process. This can include using natural light sources and avoiding artificial lighting that may introduce color distortions. Also, the camera settings such as exposure time, aperture, and focal length should be adjusted and consistent through imaging. Moreover, to ensure a more accurate comparison between the colors of the particle, the RGB values can be calculated. In the context of image analysis, RGB values are used to quantify and represent the colors of objects or pixels in an image. By measuring the RGB values of a selected area or pixel, it is possible to determine the color composition and make further color-based analyses or comparisons. (Marti et al., 2020).

The results, showing the particle projected area for each polymer type, are presented in Figures 17 to 21. This visual guide provides a clear representation of the changes in the surface area for all ten MP particles of each polymer type. The diagram shows the projected area of the particles following various treatment procedures, which include SDS treatment, protease treatment, cellulose and viscozyme treatment, Fenton oxidation treatment, and density separation utilizing SPT or $ZnCl_2$ as heavy liquids. To explore potential variations arising from the choice of liquid medium, five particles were immersed in SPT, while the remaining five particles underwent treatment using $ZnCl_2$.

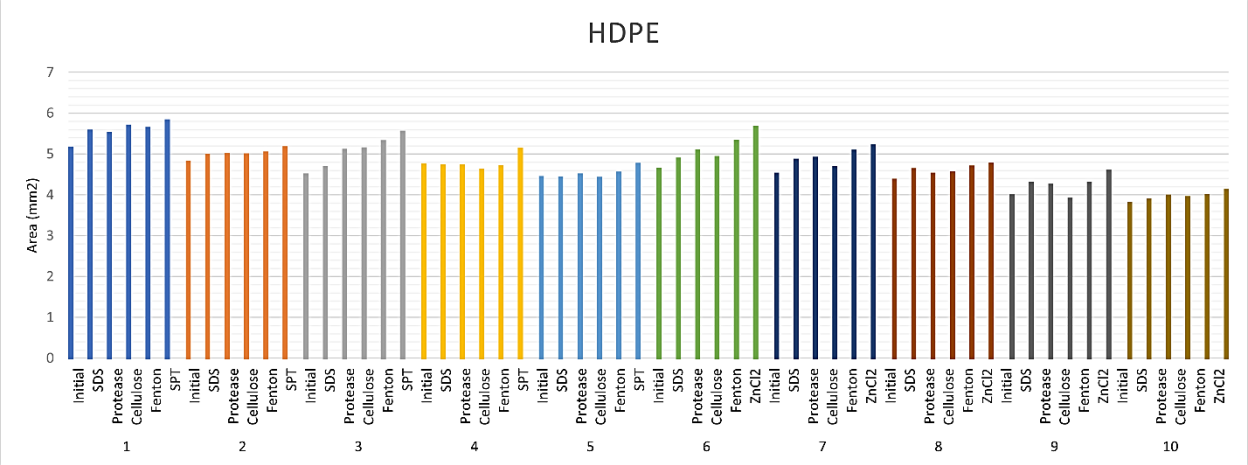

Figure 32. Diagram illustrating the initial projected area in mm² of each HDPE particle (number 1 to 10) along with the subsequent projected areas after each treatment procedure.

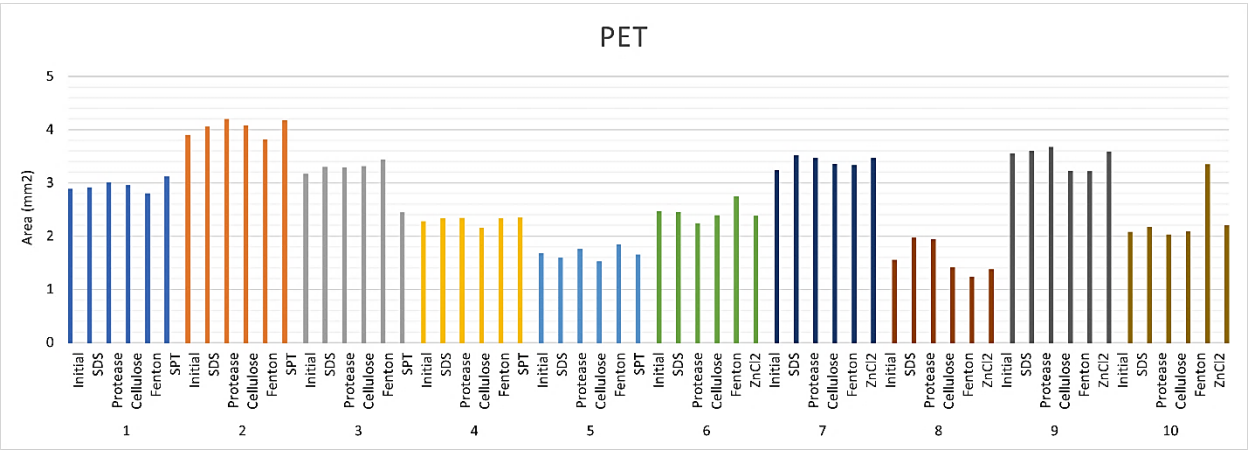

Figure 33. Diagram illustrating the initial projected area in mm² of each PET particle (number 1 to 10) along with the subsequent projected areas after each treatment procedure.

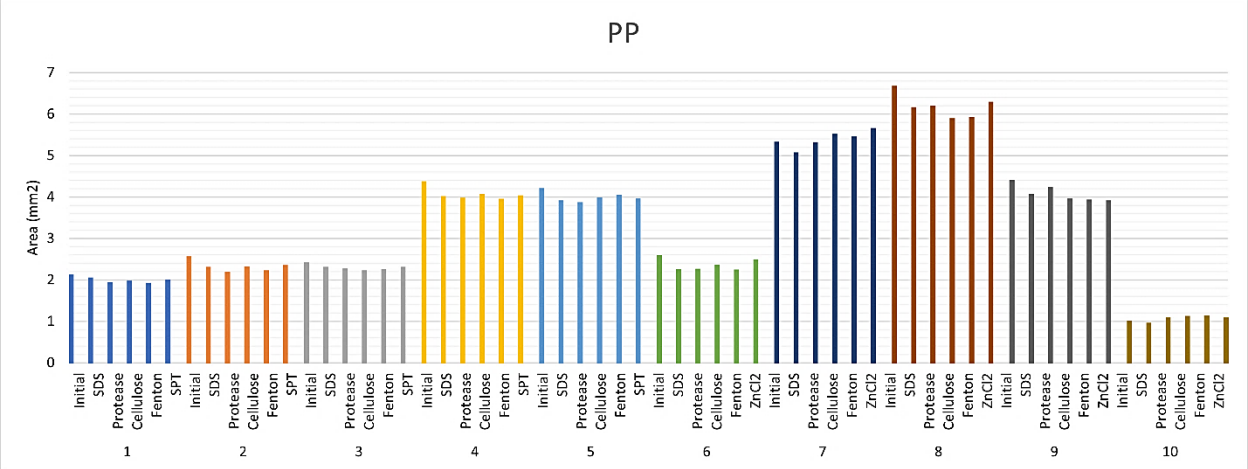

Figure 34. Diagram illustrating the initial projected area in mm² of each PP particle (number 1 to 10) along with the subsequent projected areas after each treatment procedure.

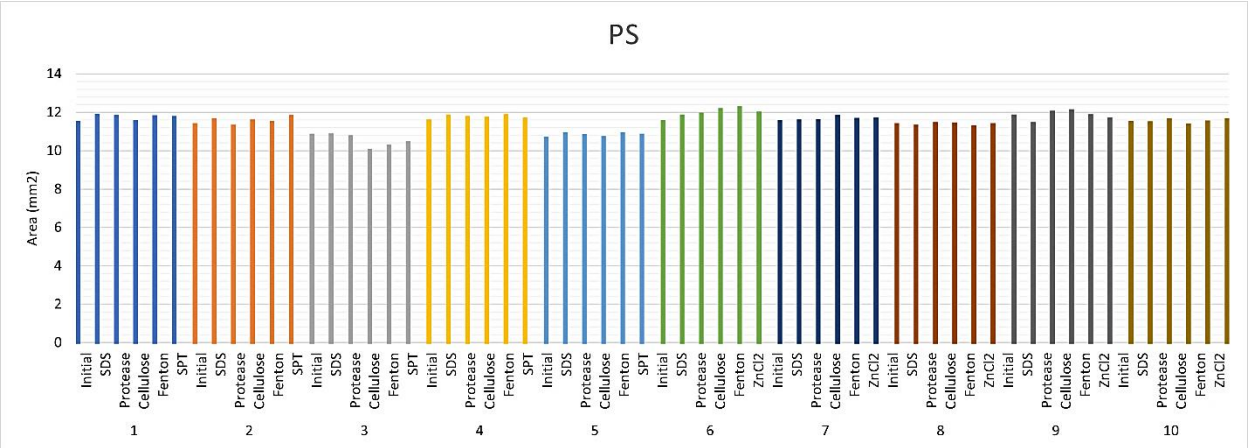

Figure 35. Diagram illustrating the initial projected area in mm² of each PS particle (number 1 to 10) along with the subsequent projected areas after each treatment procedure.

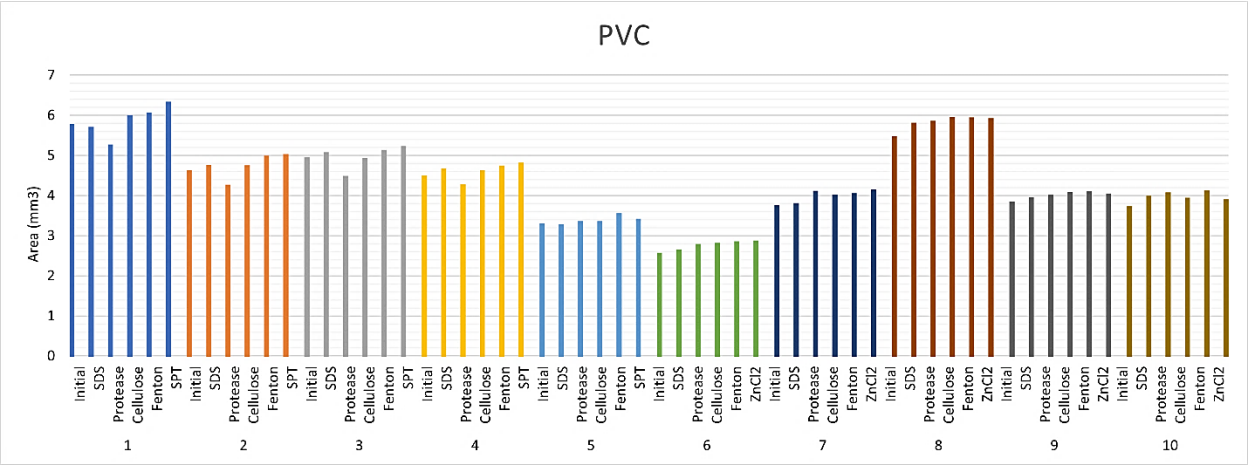

Figure 36. Diagram illustrating the initial projected area in mm^2 of each PVC particle (number 1 to 10) along with the subsequent projected areas after each treatment procedure.

Figures 17 to 21 show that there is variability in the projected area of particles at different protocol steps. For HDPE particles, the mean coefficient of variability in the projected area of all particles is 4.46%. When considering PET particles, the mean variability is higher at 8.72%, indicating a larger degree of variation in the projected areas of these particles throughout the protocol steps. For PP particles, the mean variability between areas is measured at 4.55%, while for PS particles the mean variability is 1.44%, indicating minimal changes in their projected areas throughout the protocol steps. Lastly, the mean variability of PVC particles is measured at 4.25%.

Upon closer examination of the numerical data, it becomes evident that there are fluctuations in the projected area of the particles. It is important to note that these variations are not caused by chemical influences but rather by the employed threshold technique utilized for area measurement. Relying only on the threshold method may not produce precise results due to certain limitations. One limitation is the potential misinterpretation of shadows surrounding a particle in the image, which may mistakenly be included as part of the particle itself, leading to an overestimation of the results. On the other side, in certain particle images, the threshold technique may fail to capture all the edges of the particle, resulting in an underestimation of the measured area. These factors contribute to the overall inaccuracy associated with employing the threshold method as a means of precise area determination.

Furthermore, it is noticed that some PET particles show greater variation in a projected area between the various treatment steps. This can be because of the PET particles thinness, which allows them to be flexible and adopt varying shapes. Particularly, the ends of these thin particles tend to twist and congregate, contributing to the differences in a projected area. This

is observed for particles number 3, 8, and 10 (Coefficients of variability in a projected area between protocol steps are 11.46%, 19.96%, and 22.16% respectively). For particle number 3, the initial projected area was 3.14 mm^2, which slightly increased to 3.27 mm^2 after SDS treatment, followed by a comparable projected area of 3.26 mm^2 after protease treatment. However, a significant decrease was observed after cellulose treatment, resulting in a projected area of 2.28 mm^2. Subsequently, the projected area increased to 3.42 mm^2 after the Fenton oxidation treatment, followed by a reduction to 2.42 mm^2 after density separation using SPT. Similarly, for particle number 8, the initial projected area was 1.52 mm^2, which increased to 1.94 mm^2 after SDS treatment and remained relatively consistent at 1.92 mm^2 after protease treatment. However, a noticeable decrease in the projected area was observed after cellulose and viscozyme treatment, resulting in a projected area of 1.38 mm^2. This decrease is primarily attributed to the twisting behavior of the thin particles which can be seen in Figure 22, rather than a direct chemical influence.

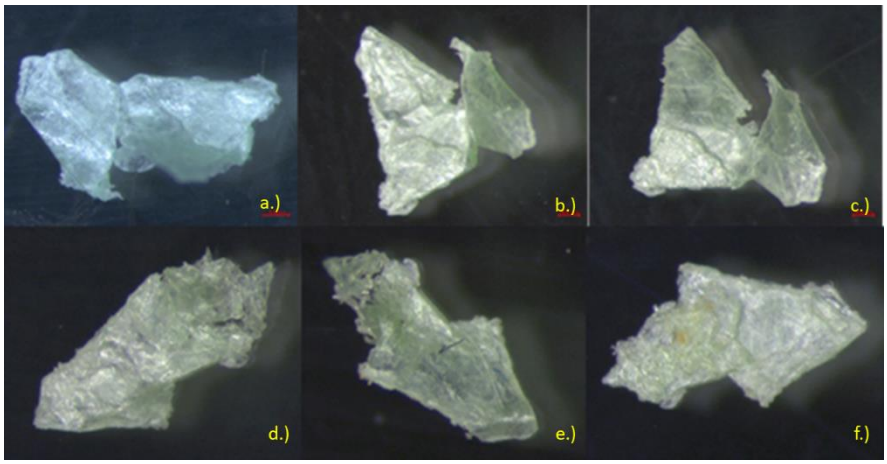

Figure 37. Microscopic images of PET particle number 8 taken before and after each of the sample preparation treatment. The initial appearance of each particle is shown in image a, while images b through f show the particles after undergoing specific treatments, including SDS (b), protease(c), cellulose and viscozyme(d), Fenton oxidation(e), and density separation (f).

Furthermore, for particle number 10, a potential outlier was identified after the Fenton oxidation treatment. The projected area of the particle increased significantly from 2.06 mm^2 before the treatment to 3.32 mm^2 after the Fenton oxidation treatment, and it decreased to 2.18 mm^2 after the subsequent density separation using $ZnCl_2$. The increase in the projected area after the Fenton oxidation treatment could be attributed to the stretching or elongation of the thin PET particle. These findings highlight the importance of considering the unique characteristics of different polymer types.

Looking at all the results presented, it can be concluded that sample preparation techniques have little impact on the morphological characteristics of the larger MP particles. The findings indicate no significant changes in the physical characteristics of the particles across all polymer types examined. These results suggest that the selected sample preparation procedures, including SDS treatment, enzyme treatment, Fenton oxidation treatment, and density separation treatment, do not introduce substantial nor systematic alterations to the morphology of the particles. The lack of significant morphological alterations shows that the structural consistency of particles and shape were maintained throughout the sample preparation procedure. However, it is worth noting that there are certain considerations to be taken into account when examining thin/film particles, as some changes in their characteristics were observed. Therefore, further research is necessary, particularly regarding the shape of these particles. Additionally, it is important to acknowledge that the measurement of particle area, while informative, provides only an indirect estimation of size and may not capture all dimensions of the particles, such as volume. Obtaining volume information would allow for a more comprehensive understanding of the particles' physical properties, including their mass.

4.1.2. Chemical Characterization

Figures 23 to 27 present diagrams illustrating Pearson correlation coefficients, showing the degree of similarity between the initial spectra and the spectra obtained after each step of the sample preparation treatment for ten particles of each polymer type (HDPE, PET, PP, PS, and PVC). To ensure accurate comparisons, the spectra underwent normalization and baseline correction to eliminate any inherent variations. Normalization was used to scale the intensity of spectral peaks to a standard range or reference point which helps to remove variations in peak intensities. Baseline correction was employed to remove background noise that can cause fluctuations in baseline spectra.

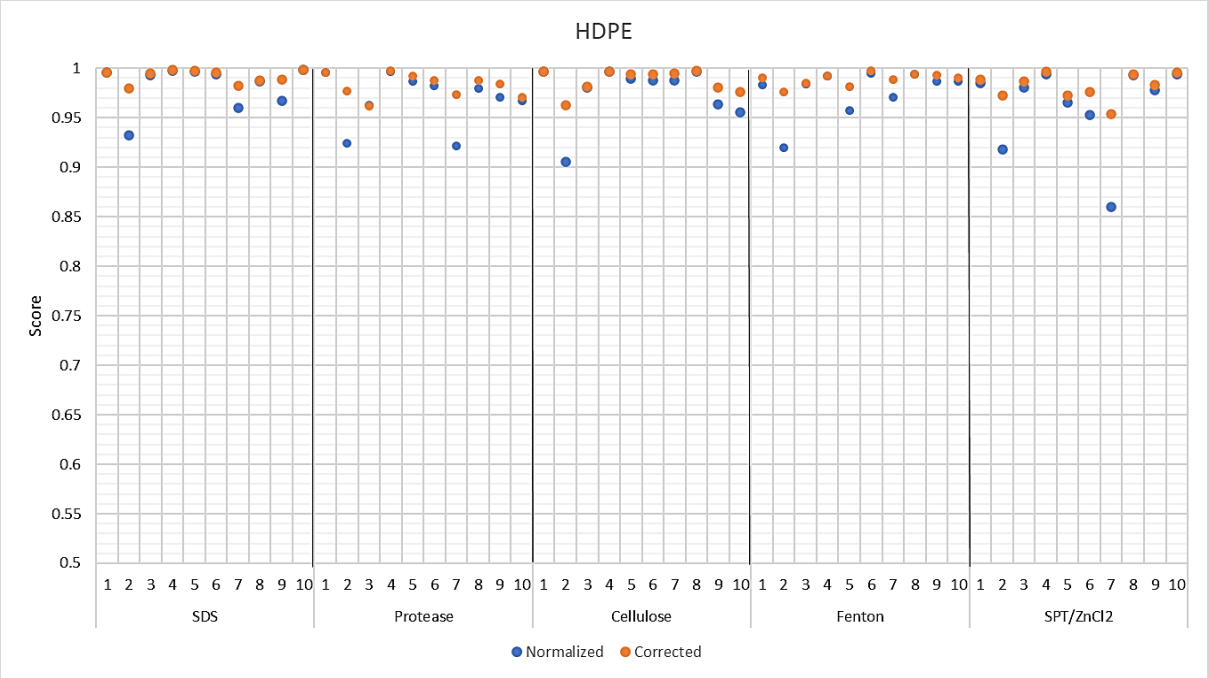

Figure 38. Pearson correlation coefficients, showing the degree of similarity between the initial spectra and the spectra obtained after each step of the sample preparation treatment for ten HDPE particles

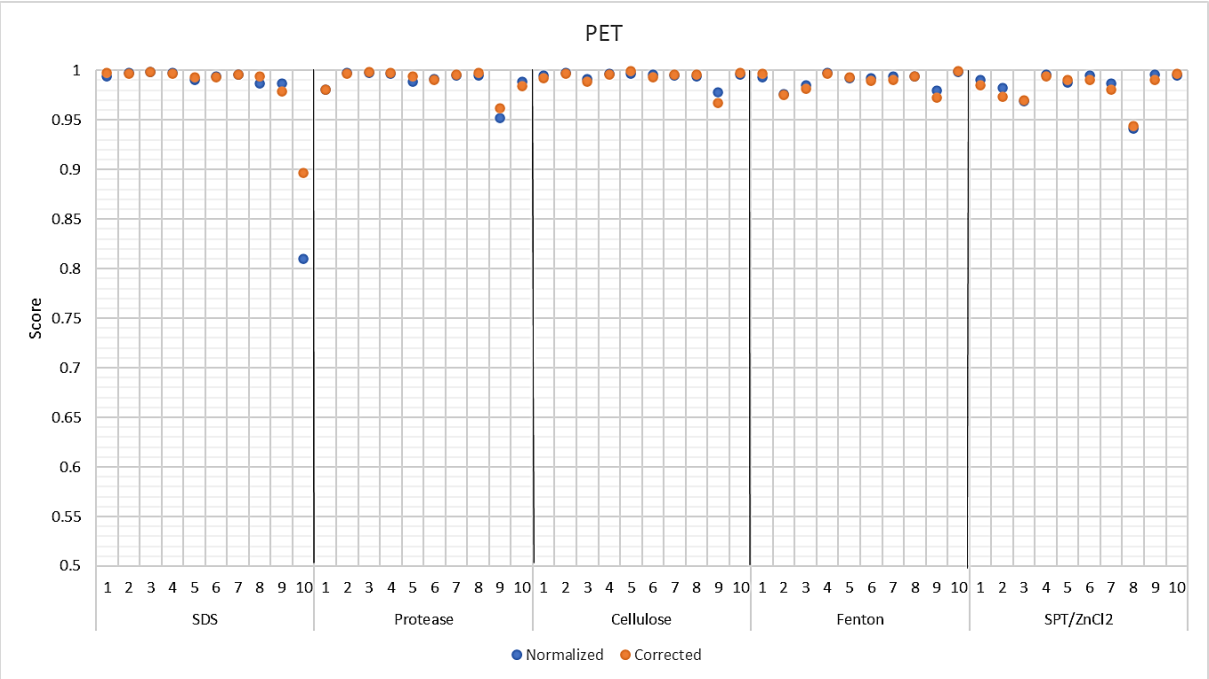

Figure 39. Pearson correlation coefficients, showing the degree of similarity between the initial spectra and the spectra obtained after each step of the sample preparation treatment for ten PET particles.

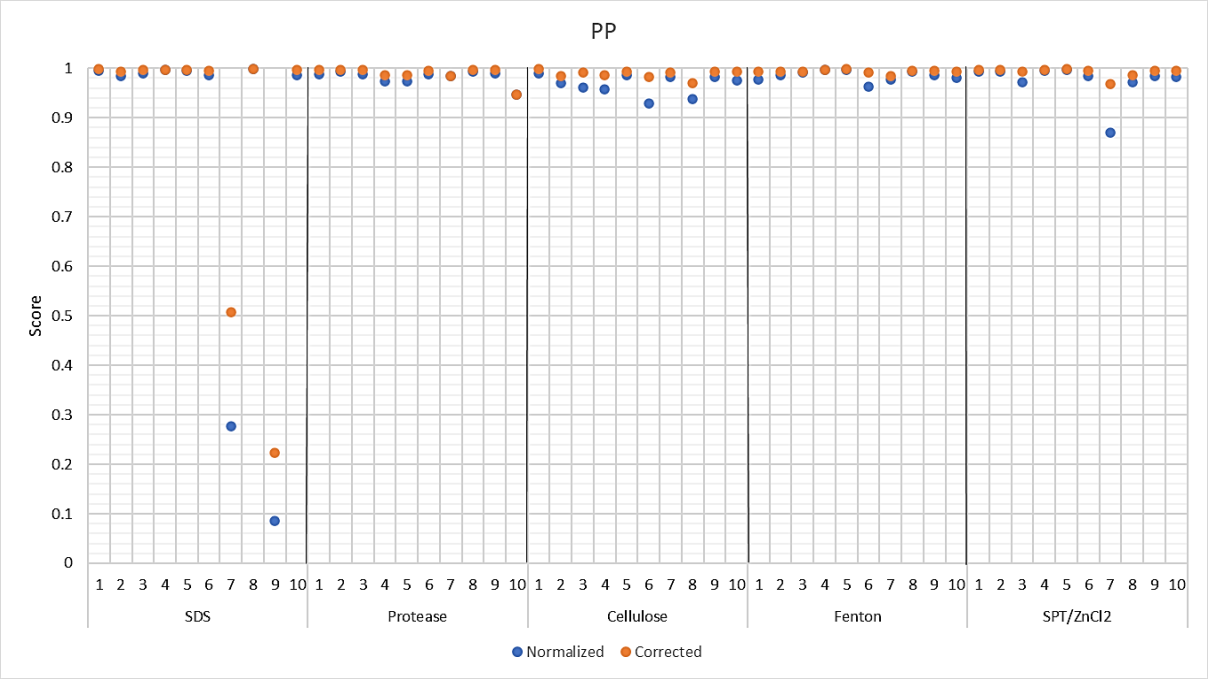

Figure 40. Pearson correlation coefficients, showing the degree of similarity between the initial spectra and the spectra obtained after each step of the sample preparation treatment for ten PP particles.

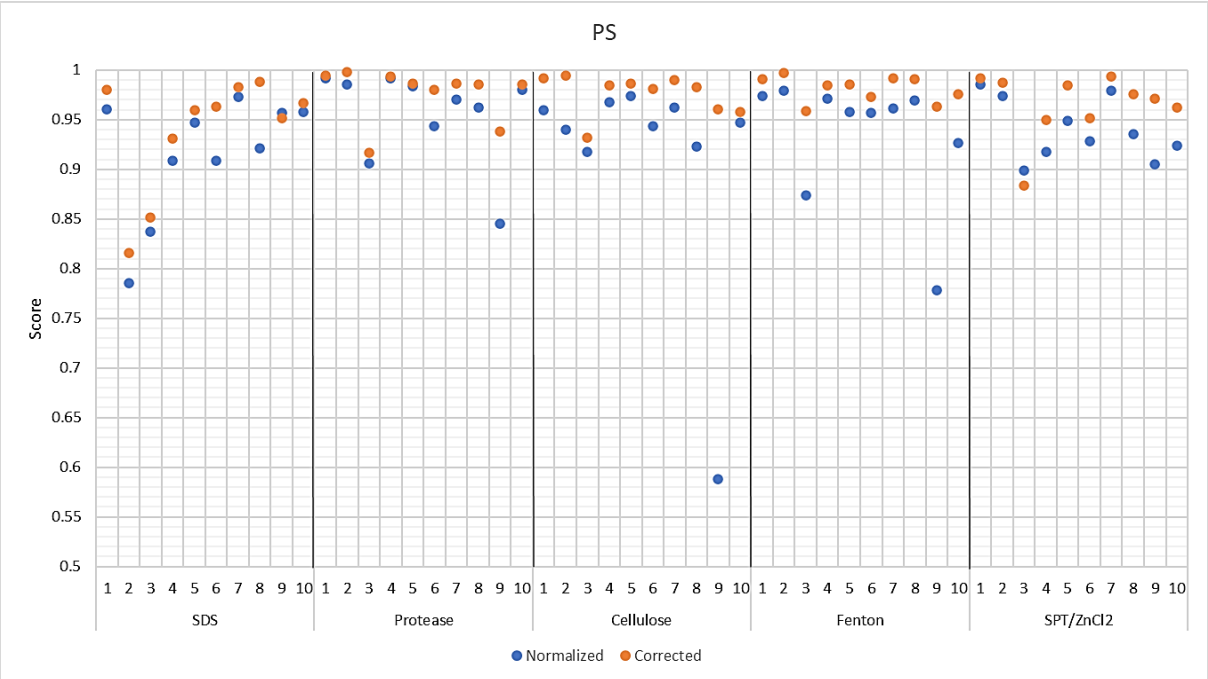

Figure 41. Pearson correlation coefficients, showing the degree of similarity between the initial spectra and the spectra obtained after each step of the sample preparation treatment for ten PS particles.

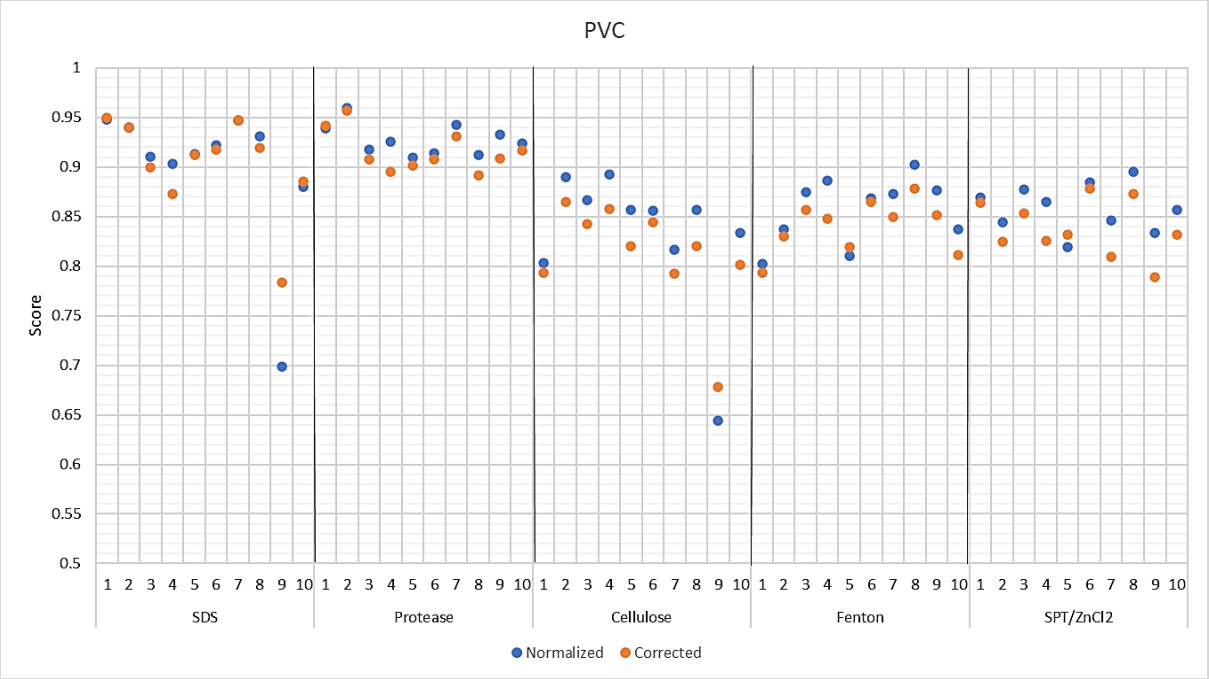

Figure 42. Pearson correlation coefficients, showing the degree of similarity between the initial spectra and the spectra obtained after each step of the sample preparation treatment for ten PVC particles.

The analysis of the results for HDPE particles indicates that there was a good match between spectra after all treatment procedures with coefficients with just normalization of the spectra ranging from 0.99 at the beginning of the protocol to 0.85 after the last step. These results were particularly evident after the application of baseline correction, where no particle had a coefficient lower than 0.95, indicating the absence of significant changes in the particle spectra. This suggests that the chemical structure of the HDPE particles remains unaffected by the chemicals applied in the sample preparation steps.

Similar observations were made for the PET particles, with consistently high match coefficients observed across all treatment procedures (from 0.99 to 0.94 with a corrected baseline). However, an outlier was identified in particle number 10 which has 0.9 match after the treatment with SDS. Further examination of the spectra revealed an additional peak, as shown in Figure 28.

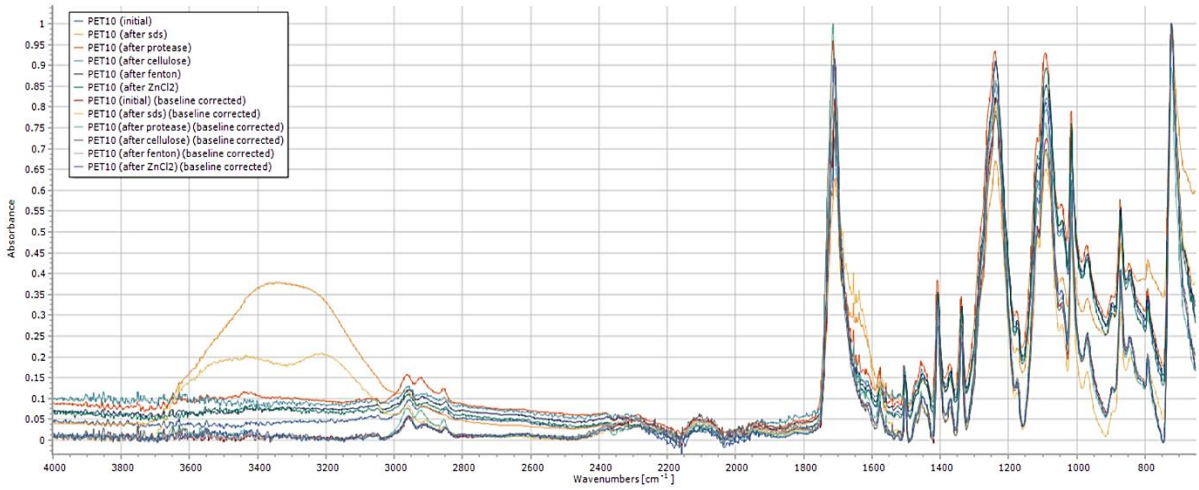

Figure 43. Spectra (normalized and baseline corrected) for PET particle number 10 showing additional peak after treatment with SDS.

The presence of an additional peak in the wavenumber range of 3600 to 3000 cm^{-1} was noticed in the spectra of particle number 10 after the SDS treatment, even after normalization and baseline correction. This suggests the potential presence of chemical residue on the particle because of the inadequate rinsing with water during the filtration step following the SDS treatment, rather than attributing it as a direct impact of the SDS on altering the chemical structure of the particle.

Similarly, the PP particles demonstrated high Pearson's correlation coefficients after all sample preparation procedures, ranging from 0.99 to 0.95 indicating no changes in their chemical composition. Still, two outliers were noticed in particle numbers 7 and 9 with matching coefficients of 0.51 and 0.22 respectively. Similar to the case of PET particle number 10, these outliers can be attributed to the presence of SDS residues on the particles. The corresponding spectra in Figures 29 and 30 demonstrate the appearance of additional peaks, further supporting this observation.

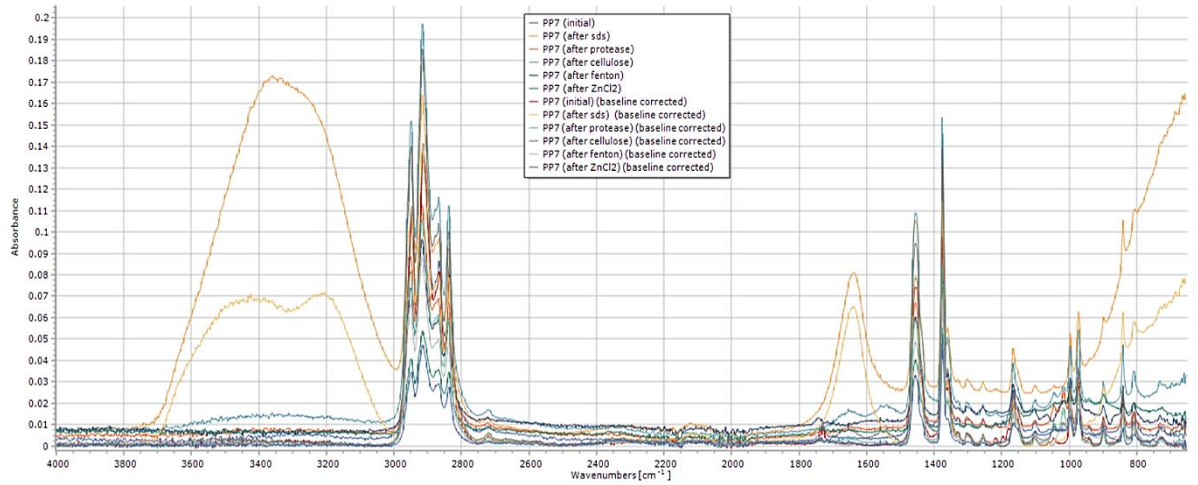

Figure 44. Spectra (normalized and baseline corrected) for PP particle number 7 showing two additional peaks and high peak intensity after treatment with SDS.

Figure 29 shows the appearance of the same peak in PP particle number 7 as in the case of PET particle number 10. This peak is located in the wavenumber range between 3800 and 3000 cm^{-1}. Additionally, in this PP particle, an extra peak appears in the wavenumber range between approximately 1700 and 1500 cm^{-1}. Moreover, the very high intensity of the peak is noticed at the end of the spectra. These additional peaks are only detected after the SDS treatment and not observed during subsequent treatments, indicating their association with inadequate water rinsing during filtration and the presence of SDS chemical residues on the surface of the particle. Figure 30 illustrates a similar scenario for PP particle number 9.

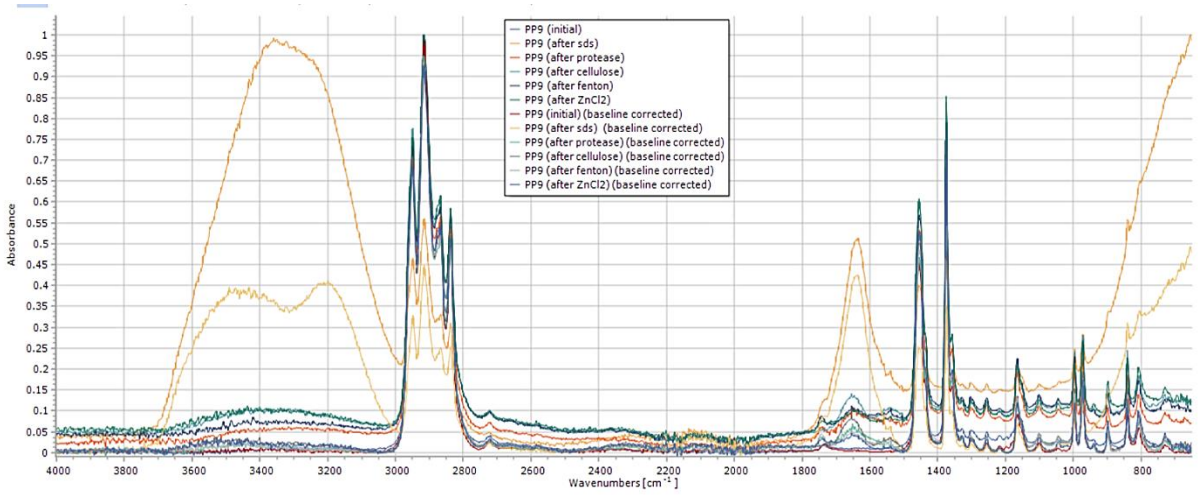

Figure 45. Spectra (normalized and baseline corrected) for PP particle number 9 showing two additional peaks and high peak intensity after treatment with SDS.

Upon closer examination of the PS particles, there is a slight overall decrease in Pearson's correlation coefficient scores. However, it is important to note that even with the lower overall coefficients ranging between 0.58 and 0.9, after the application of baseline correction, all particles exhibited coefficients no lower than 0.9 except two outliners in particle number 2 and 3 after the SDS treatment with matching coefficients of 0.82 and 0.85 respectively, which is also explained with the appearance of the peak from SDS residuals, so it can be concluded that there are no significant changes in the chemical structure of the PS particles throughout the sample preparation procedures.

Looking at coefficients for PVC particles, a decrease in the coefficient score was noticed across all PVC particles, from 0.95 to 0.78 (excluding the outliner in particle number 9 after SDS and Cellulose treatment). By the completion of the treatment, after the last protocol step (density separation), the coefficients for all ten particles ranged between 0.78 and 0.87, which, compared to the other polymers investigated, represented a lower score. The lower coefficient scores could potentially be attributed to variations in the intensity of the spectra peaks, even after applying normalization and baseline correction techniques. This variation is shown in Figure 15. However, it is noteworthy that even after undergoing treatment with SDS, there is a persistent bump in the 3600-3000 cm^{-1} region for PVC particles, unlike the other polymers. This observation suggests that the change in PVC particles is consistent and not fully eliminated in the subsequent steps of the protocol. As a result, it contributes to a lower matching index, indicating a weaker similarity between the treated PVC particles and the reference spectra. For a deeper understanding, further analysis of the PVC spectra should be investigated to identify the specific regions within the spectra where changes occur, in order to determine if there are any particular parts of the chemical structure of PVC particles that are being affected.

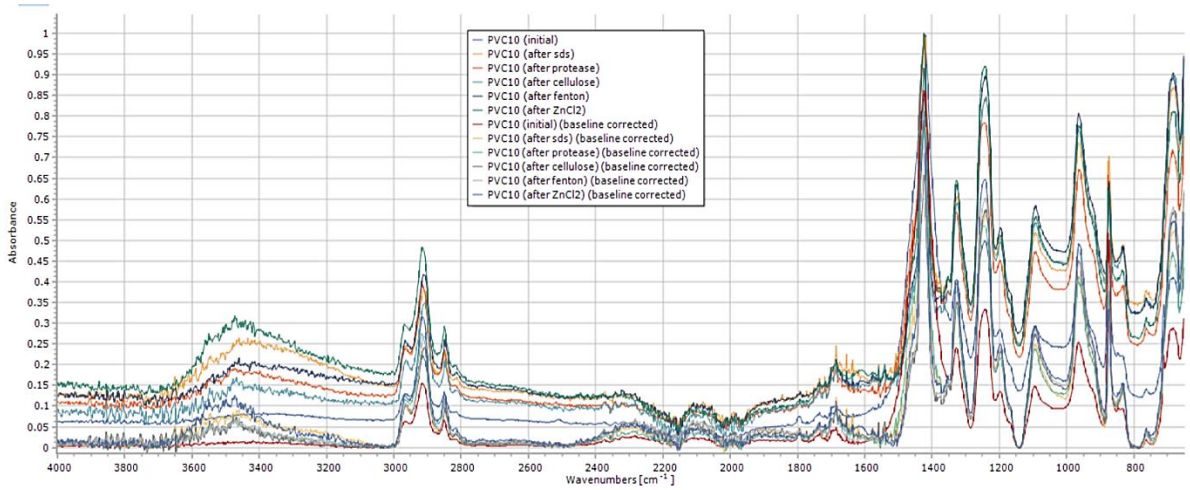

Figure 46. Spectra (normalized and baseline corrected) for PVC particle number 10.

Figure 31 illustrates the presence of varying peak intensities, which could potentially contribute to a lower match in spectra in PVC particles. This intensity variation is observed across all particles, making it a representative example.

The thorough examination of all particle spectra and numerical analyses strongly indicate that the chemicals and techniques utilized in the sample preparation did not significantly impact the morphological and chemical structure of the examined MP particles. This outcome can be considered favorable for a well-designed sample preparation protocol. The findings provide strong support for the ability of the implemented protocol to maintain the properties of the particles, resulting in more precise, trustworthy, and representative results from the subsequent analysis. By demonstrating that the sample preparation has minimal impact on the properties of the particles, the validity and integrity of the analysis are preserved. However, based on the presented results, it was observed that all outliers with a lower matching index were specifically associated with SDS treatment. To ensure that particles are free from SDS residues, it is crucial to thoroughly filter the treated particles with an abundant amount of particle-free water or ethanol. This finding highlights the importance when considering the use of SDS as the only treatment in sample preparation for subsequent analysis.

4.2. Comparison Between µFT-IR and Raman Spectroscopy

For particle analysis, two widely employed techniques, FPA-µFT-IR imaging and Raman spectroscopy, were explored following the laboratory treatment of the smaller MP particles (3-200 µm). As described in Chapter 3.2.1, the experimental procedure involved the preparation of a mixed solution consisting of HDPE, PET, PP, PS, and PVC polymers, comprising small MP particles. Figures 32 to 34 provide a visual representation of the results obtained from detecting particles of each polymer type using both Raman and µFT-IR spectroscopy, along with the total number of particles. These figures offer valuable insights into the detection efficiency of the two techniques and the overall distribution of particles among different polymer types. The analysis of figures reveals interesting patterns regarding the detection of MP particles using µFT-IR and Raman spectroscopy in the samples examined. In sample 1, µFT-IR detected 18 more MP particles compared to Raman, while in sample 2, there was a difference of 15 particles in favor of µFT-IR. Conversely, in sample 3, Raman detected a higher number of particles, with a total of 86 more particles than µFT-IR. This high difference can be attributed to the significant presence of PVC particles detected, as Raman detected 216 PVC particles compared to 130 detected by µFT-IR. Considering the different polymer types, Raman consistently detected a higher number of PE particles across all three samples, with an average difference of 32.2 particles. On the other hand, µFT-IR exhibited higher detection of PET particles, with an average of 75.6 more particles identified across the three samples. Regarding PP particles, Raman spectroscopy detected an average of 15 more particles, while a similar trend was observed for PS particles, with Raman detecting an average of 6.3 more particles. These findings remained consistent across all three samples, with the exception of sample 1, where µFT-IR detected 6 more PVC particles compared to Raman spectroscopy. However, in samples 2 and 3, Raman spectroscopy detected significantly more PVC particles (41 and 87 more particles, respectively) compared to µFT-IR.

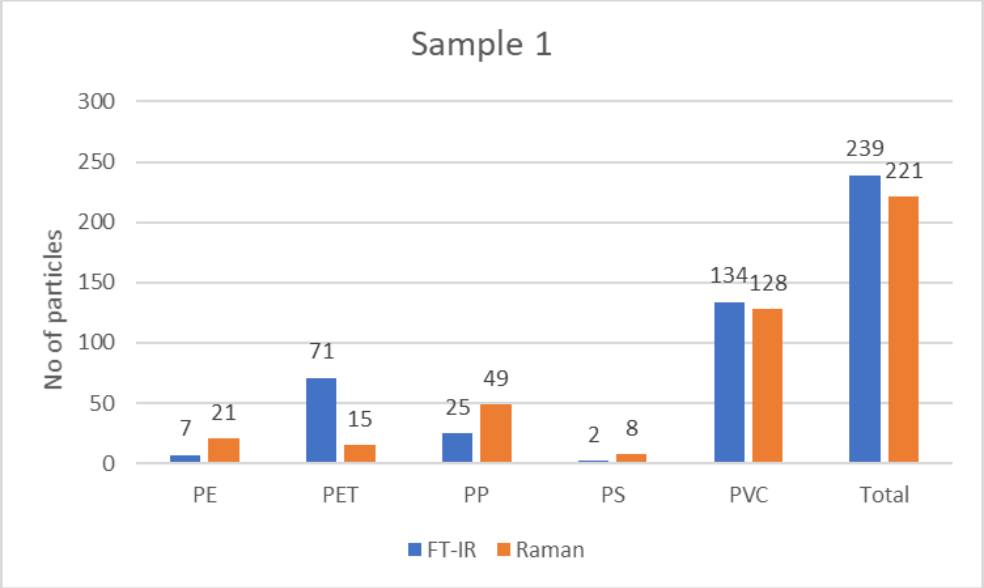

Figure 47. Comparison of particle detection using µFT-IR and Raman spectroscopy; Distribution of detected particles by polymer type in sample 1.

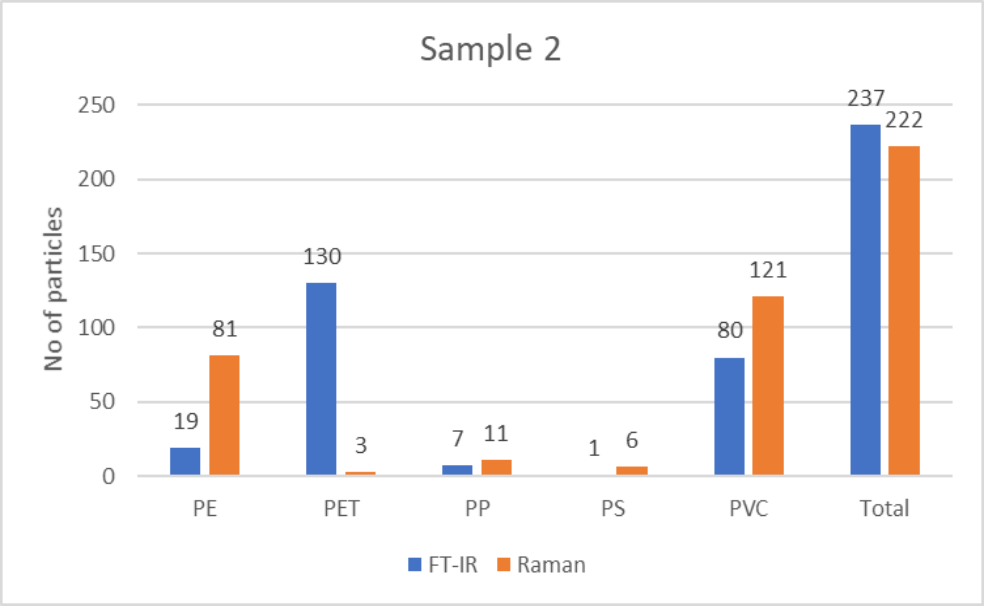

Figure 48. Comparison of particle detection using µFT-IR and Raman spectroscopy; Distribution of detected particles by polymer type in sample 2.

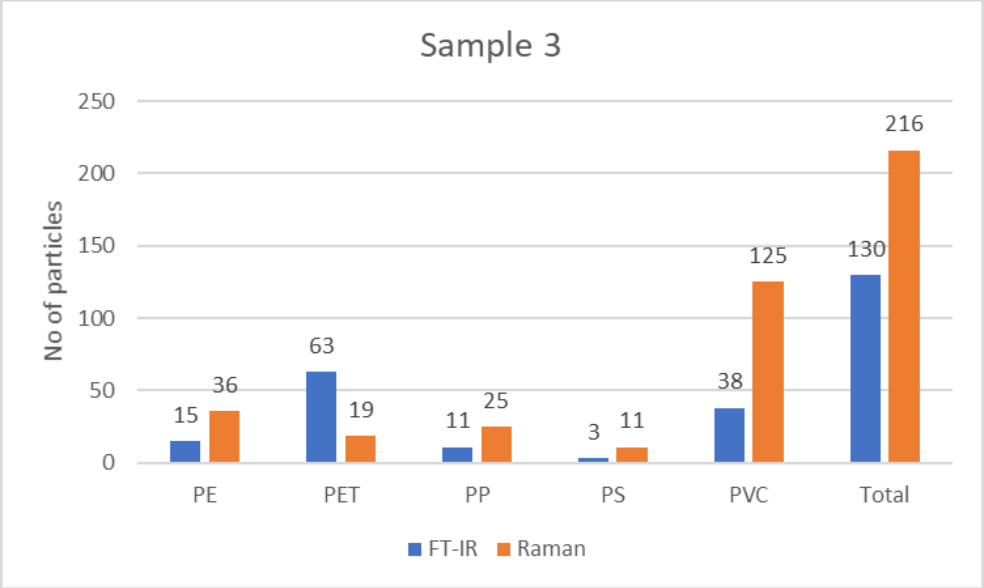

Figure 49. Comparison of particle detection using µFT-IR and Raman spectroscopy; Distribution of detected particles by polymer type in sample 3.

The results indicate that the µFT-IR and Raman spectroscopy techniques provided different results when identifying particles in the same sample. This trend was consistent across all three samples examined. However, a consistent pattern emerges in particle detection across the samples. For PE particles, Raman analysis consistently identified a greater number of particles compared to µFT-IR, whereas the reverse was observed for PET particles. In the case of PS, PP, and PVC particles, Raman spectroscopy exceeded µFT-IR in particle detection. To investigate this, a matching index between particle spectra and reference spectra was calculated to determine which technique achieved better spectral alignment. The index was computed using siMPle software that employed Pearson correlation to assess the spectral fit for untreated data, as well as its first and second derivatives. The mean matching coefficients for all polymer types obtained from µFT-IR and Raman scanning are summarized in Table 2.

Table 5. Comparison of matching index between particle spectra and reference spectra detected by µFT-IR and Raman.

	Match Coefficient							
	Sample 1		Sample 2		Sample 3		Average	
Polymer	**µFT-IR**	**Raman**	**µFT-IR**	**Raman**	**µFT-IR**	**Raman**	**µFT-IR**	**Raman**
PE	0.93	0.80	0.91	0.73	0.94	0.74	0.93	0.76
PET	0.86	0.63	0.86	0.56	0.85	0.78	0.86	0.66
PP	0.90	0.90	0.87	0.83	0.94	0.76	0.90	0.83
PS	0.90	0.90	0.89	0.79	0.83	0.69	0.87	0.85
PVC	0.75	0.72	0.75	0.67	0.75	0.68	0.75	0.69

The analysis of Pearson's correlation coefficient between particle spectra and reference spectra reveals that µFT-IR consistently showed higher matches across all particles, with an average match index of 0.86, compared to 0.76 for Raman spectroscopy. Additionally, µFT-IR detected a greater number of particles across the three samples. Because of this, µFT-IR was chosen as the preferred analysis technique to implement after the sample preparation treatment procedures. However, further investigation is necessary to examine all particle spectra and ascertain the underlying reasons for the high differences in particle detection between µFT-IR and Raman. In Figure 35, examples of low matches between particle spectra from sample 3 (for PVC, PE, PS, and PP) and the reference spectra from the Raman library are depicted. This demonstrates that although the software identified these particles, it is necessary to verify the spectra of the detected particles, particularly when they show a low matching score.

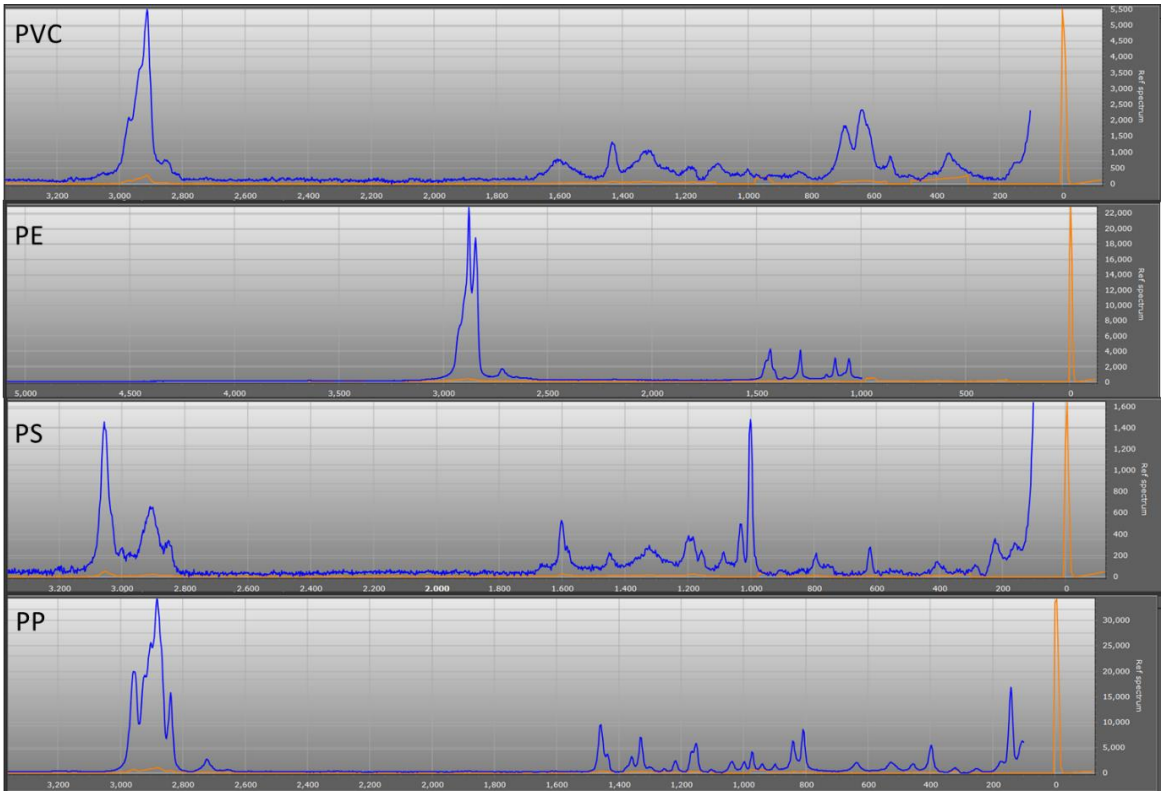

Figure 50. Low matches between particle spectra from sample 3 (for PVC, PE, PS, and PP) and the reference spectra from the Raman library

While it is true that µFT-IR exhibited better spectral matching for particles, it is important to acknowledge that the matching index depends upon the quality of the spectra. Several variables, including the analysis's setting parameters and the particle size, can significantly influence the spectra's quality. Furthermore, it is important to note that different reference spectra libraries were used, potentially contributing to the differences and highlighting the need to ensure accuracy in the reference spectra employed for Raman analysis. Another reason influencing the decision to not utilize Raman spectroscopy for particle detection is the presence of chemical residues and cellulose contamination after the treatment, as detailed in the next chapter. These interferences significantly increase the number of particles in the sample and would require considerable time for Raman spectroscopy to accurately identify the particles and compare the results before and after implementing protocol procedures.

4.3. Recovery Rate and Distribution of Small MP Particles (3 - 200µm) After Sample Preparation

Figures 36 to 40 present the particle counts before and after the sample preparation treatment along with maps of the particle distribution before and after each protocol step conducted with siMPle software.

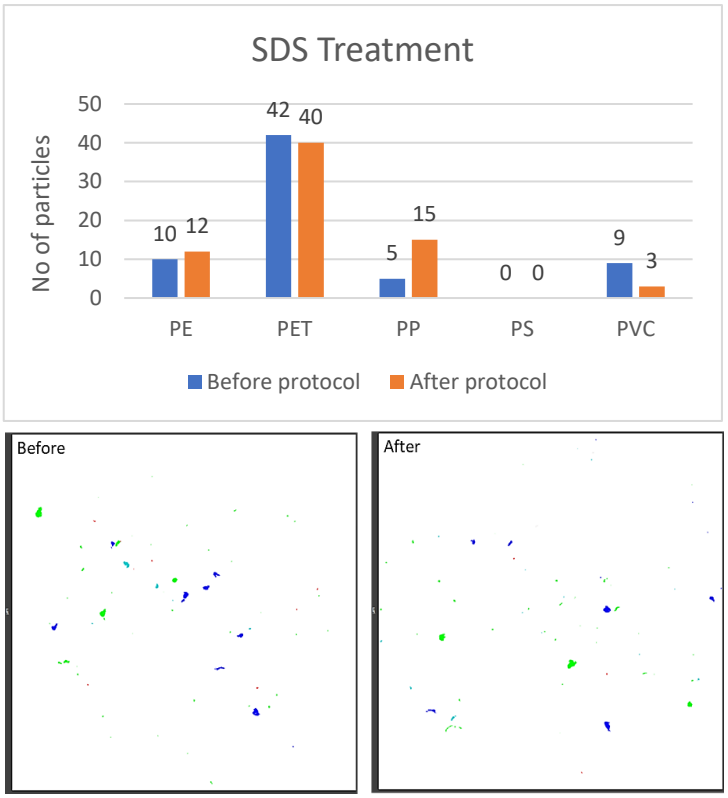

Figure 51. Particle quantification with map conducted in siMPle software: pre- and post- SDS treatment.

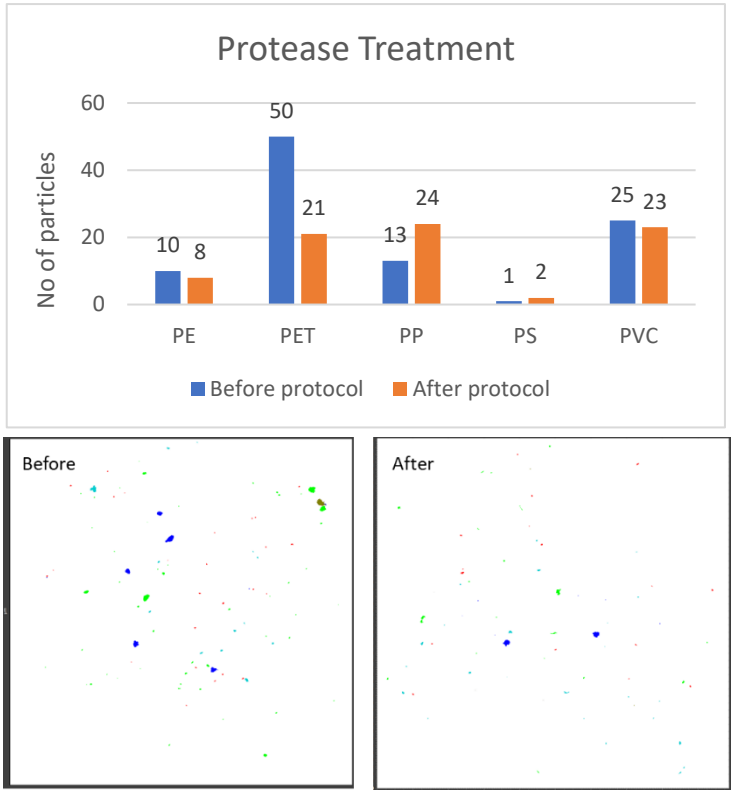

Figure 52. Particle quantification with map conducted in siMPle software: pre- and post- Protease treatment.

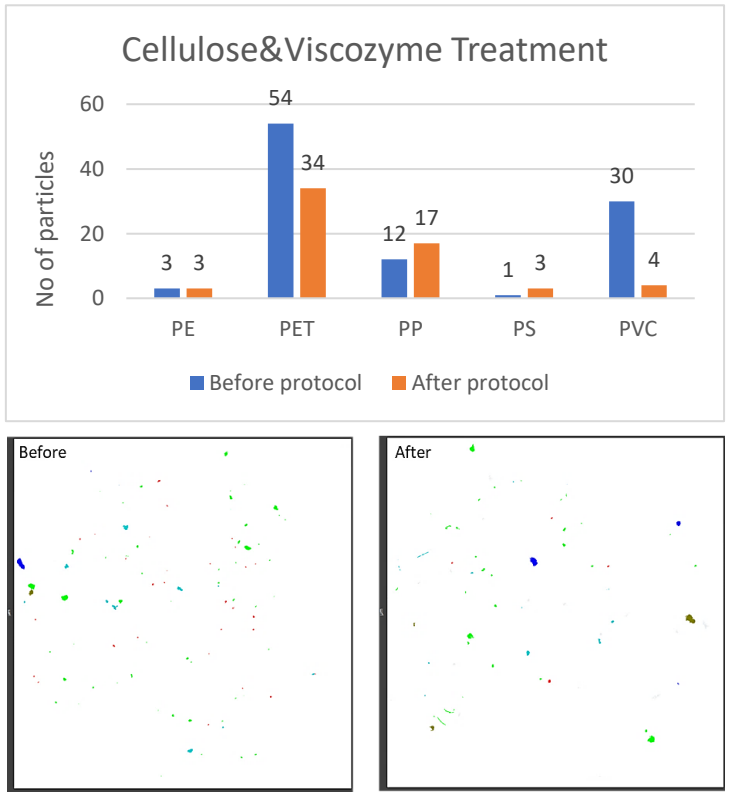

Figure 53. Particle quantification with map conducted in siMPle software: pre- and post- Cellulose and Viscozyme treatment.

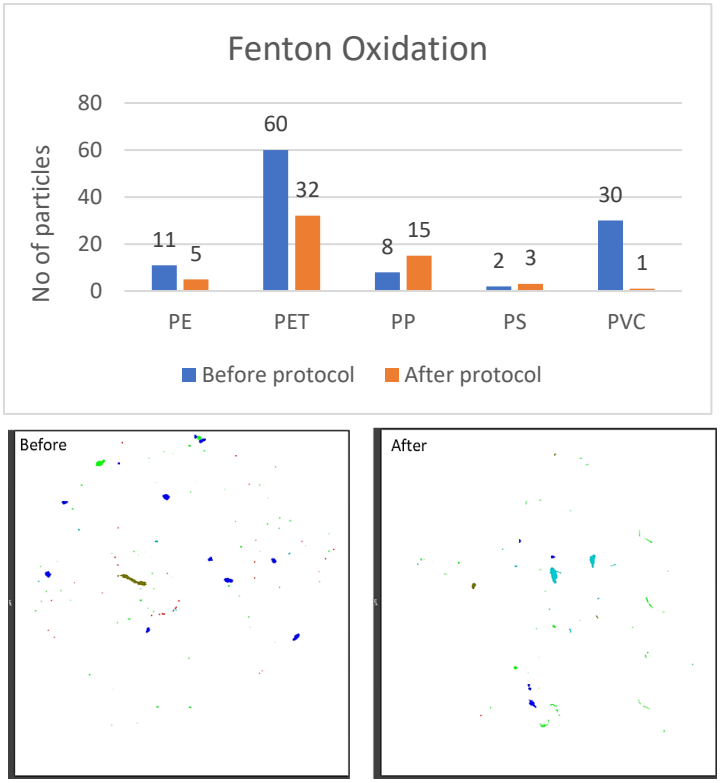

Figure 54. Particle quantification with map conducted in siMPle software: pre- and post- Fenton oxidation.

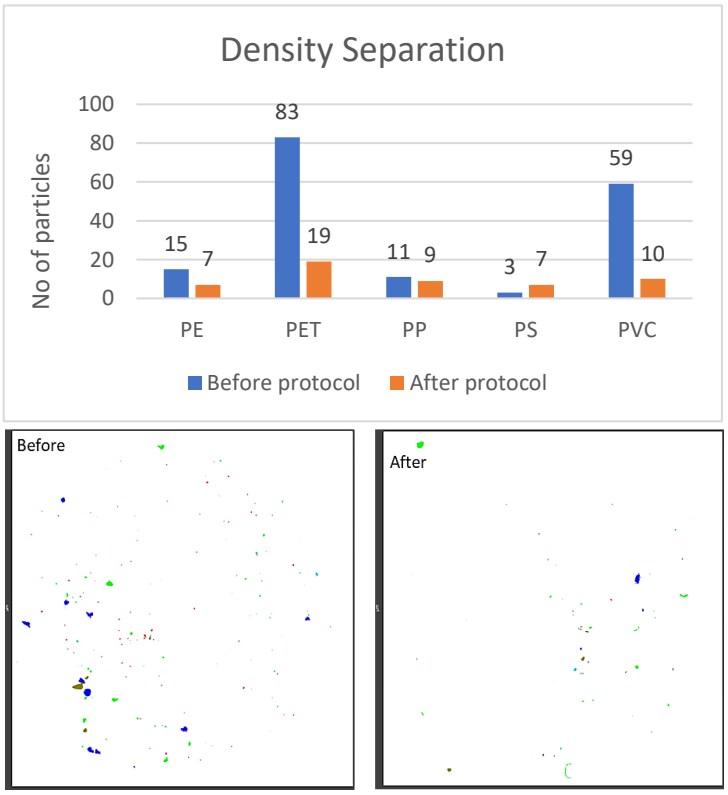

Figure 55. Particle quantification with map conducted in siMPle software: pre- and post- Density separation.

Examining the figures and particle recovery rates (Table 3.) reveals that the overall recovery was not optimal. As the protocol progressed, the recovery rates declined. The lowest recovery rate across all treatments was observed for PVC particles (SDS: 33.3%, Cellulose and Viscozyme: 13.3%, Fenton: 3.3%, Density separation: 16.9%) except Protease (92.0%), likely due to their small size (20-40 µm), making them prone to being masked by chemical residues or potentially lost during the sample preparation process prior to scanning. Additionally, there was a consistent decline in the recovery of PET particles throughout the procedure (SDS: 95.2%, Protease: 42.0%, Cellulose and Viscozyme: 63.0%, Fenton: 53.3%, Density separation: 22.9 %). Notably, visual differences were observed in the samples before and after treatment. Despite filtering the samples with a 10 µm mesh prior through the same membranes used for deposition, traces of chemical residues and fiber contamination remained, potentially originating from airborne sources. These contaminants could interfere with the µFT-IR scanning, obstructing the signal from MP particles and resulting in lower identification rates post-treatment. The heavy presence of chemical residues and contamination was primarily attributed to filtering the whole amount of the samples back onto the silicone membrane for scanning to evaluate the effectiveness of this preparation approach. Figure 41 illustrates the visual appearance of the samples after the sample preparation protocol, together with a map obtained from µFT-IR analysis. The grey particles depicted in the map represent cellulose fibers that were detected using µFT-IR.

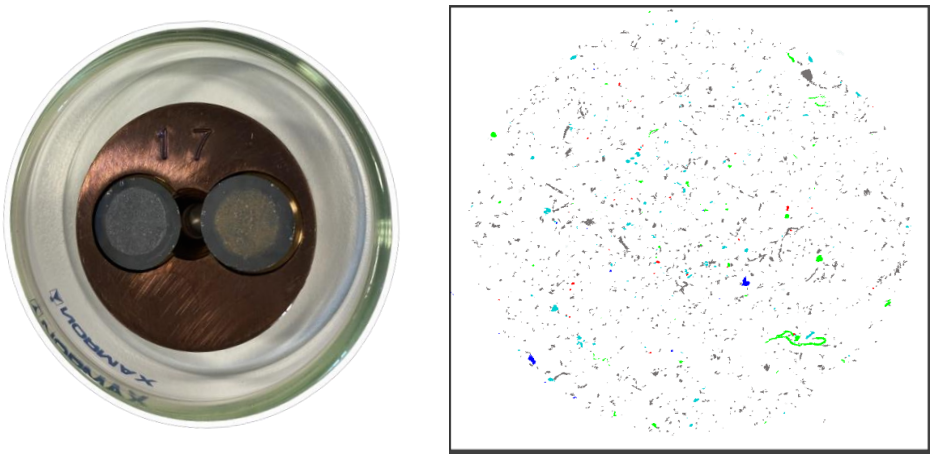

Figure 56. Visual appearance of the sample after the treatment implementation and FT-IR scan mapping of the sample including cellulose fibers.

To avoid such issues, the standard procedure involves complete evaporation of the samples in glass vials after the final treatment step, followed by the addition of a known amount of ethanol to prepare the samples for scanning. Depending on the appearance of the sample,

only a representative portion is deposited and scanned, ensuring a more accurate analysis. The presence of contamination in the samples requires careful consideration when conducting scanning procedures, particularly when dealing with samples that may contain a substantial amount of matrix such as soil or sediments, where the possibility of residual contamination traces is high, given the difficulty of completely removing all organic or inorganic particles from MP samples. After evaporation, a representative portion of the sample can be deposited and scanned, ensuring that the particles are spread out and less likely to be obscured by non-MP particles. By depositing a smaller portion, the chances of detecting and identifying MP particles with higher accuracy are improved. Moreover, careful attention to the visual appearance of the samples before proceeding with the scanning process and the implementation of robust filtration techniques will further contribute to improving the overall analysis quality. Despite prior filtration of the samples using a ø 47 mm 10 µm mesh filter followed by filtering through ø 13 mm 5 µm mesh silicone membranes, residual contaminants were still present. To further improve the removal of these residues, an additional filtration step using a ø 47 mm with 5 µm mesh filter could be incorporated. The larger filtering surface area of the ø 47 mm filter would contribute to reducing contamination levels from chemical residues. This additional filtration step can be implemented as part of the sample preparation protocol to ensure more thorough removal of contaminants and enhance the overall quality of the analysis. These measures are important steps toward obtaining more accurate and reliable results in MP research.

Table 6. Recovery rates for small MP particles together with the average value for recovery rate per protocol step.

	Recovery rate, %				
Polymer	**SDS**	**Protease**	**Cellulose and Viscozyme**	**Fenton**	**Density separation**
PE	120.00	80.00	100.00	45.45	46.67
PET	95.24	42.00	62.96	53.33	22.89
PP	300.00	184.62	141.67	187.50	81.82
PS	/	200.00	300.00	150.00	233.33
PVC	33.33	92.00	13.33	3.33	16.95
Average	137.14	119.72	123.56	87.92	80.33

On the other side, looking at the table it could be noticed an increase of particles in some treatments. Results from recovery rates reveal an increase in the particle count for PE particles

following the SDS treatment (120%). Furthermore, for PP particles, a rise in a count is observed after all treatments except for density separation (SDS: 300 %, Protease: 185 %, Cellulose and Viscozyme: 142 %, and Fenton: 188 %) Similarly, for PS particles, an increase in count is noticed following each treatment (Protease: 200%, Cellulose and Viscozyme: 300 %, Fenton: 150 %, and Density separation: 233 %) excluding SDS treatment because no PS particles were detected prior no after the treatment. To investigate the potential cause of this, the size distribution of these particles was examined, to determine if any changes in particle size occurred during the treatments that could contribute to the higher particle counts. Figures 42 to 50 present the histograms of the size distribution of these particles for providing insights into the potential presence of smaller particles after treatment, resulting from the possible breakage of particles during the sample preparation.

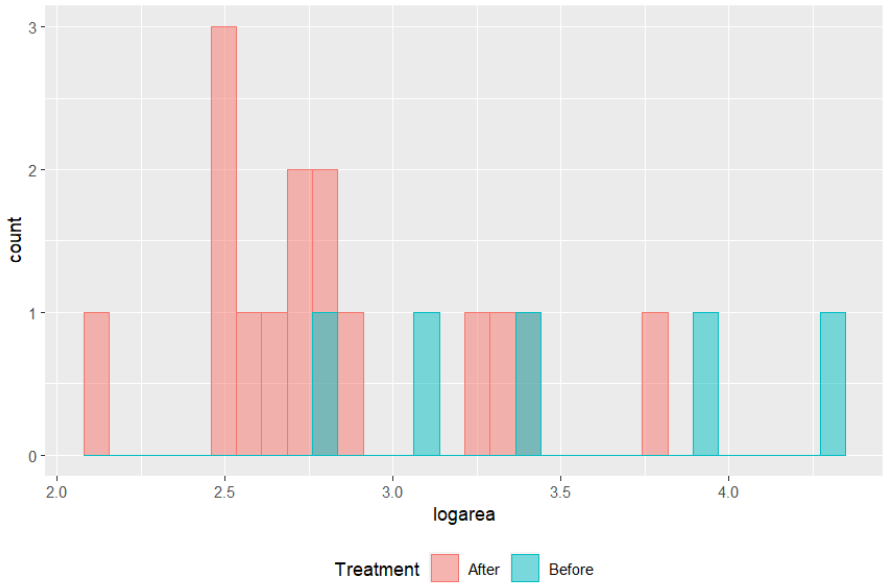

Figure 57. Size distribution of PP particles before and after SDS treatment.

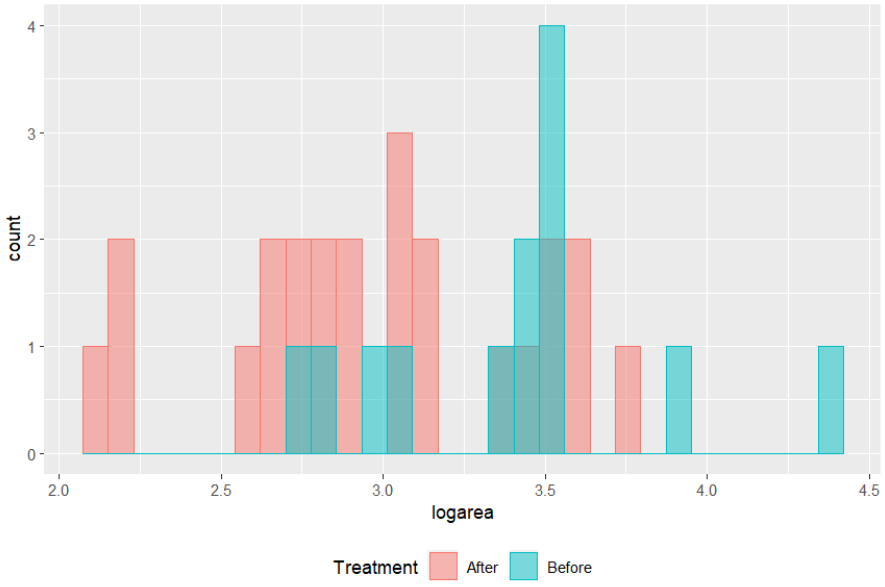

Figure 58. Size distribution of PP particles before and after Protease treatment.

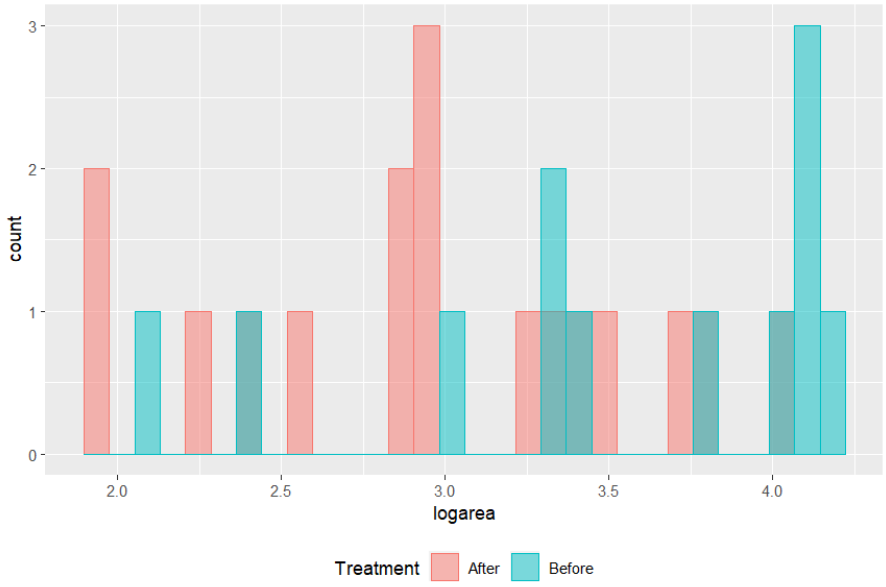

Figure 59. Size distribution of PP particles before and after Cellulose and Viscozyme treatment.

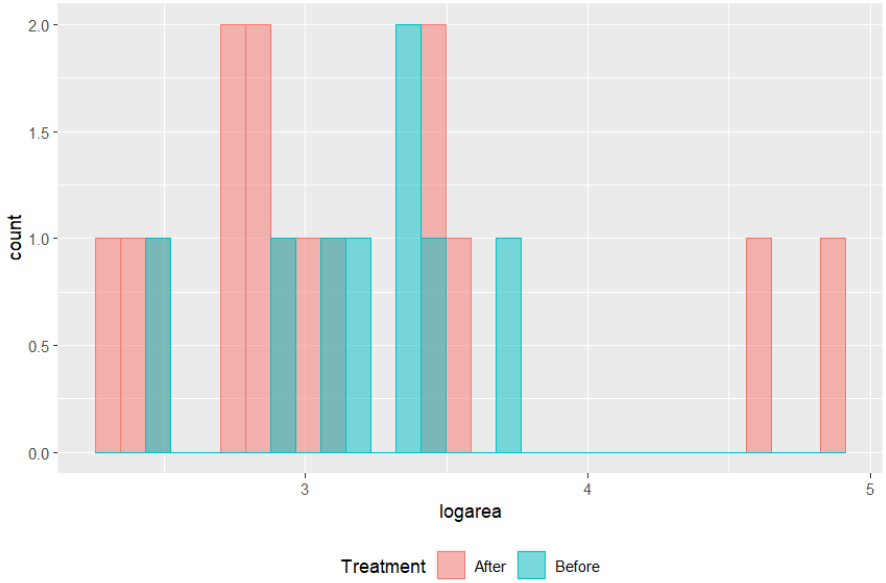

Figure 60. Size distribution of PP particles before and after Fenton oxidation.

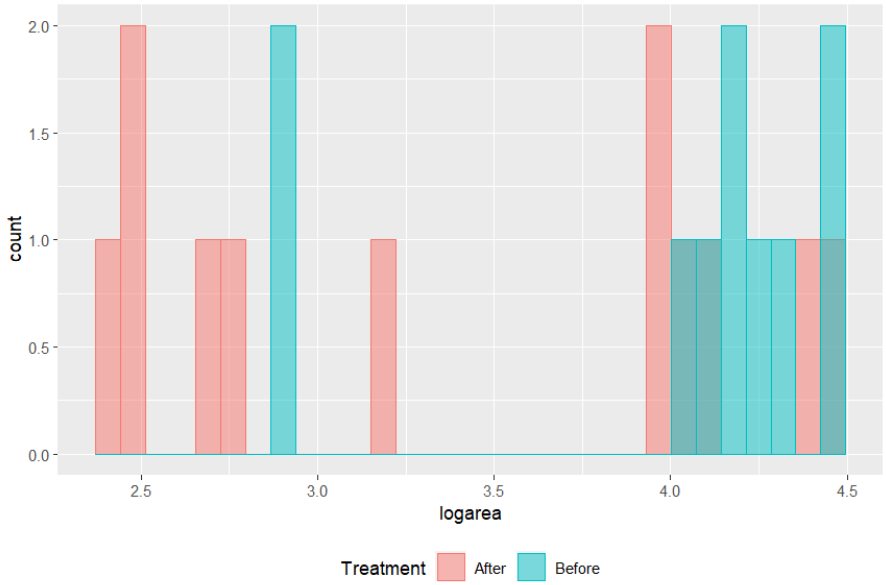

Figure 61. Size distribution of PE particles before and after SDS treatment.

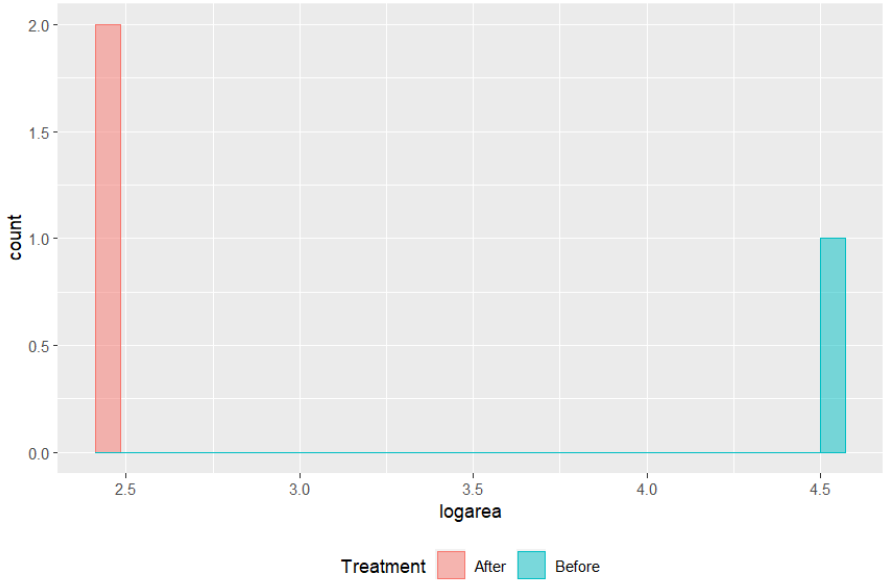

Figure 62. Size distribution of PS particles before and after Protease treatment.

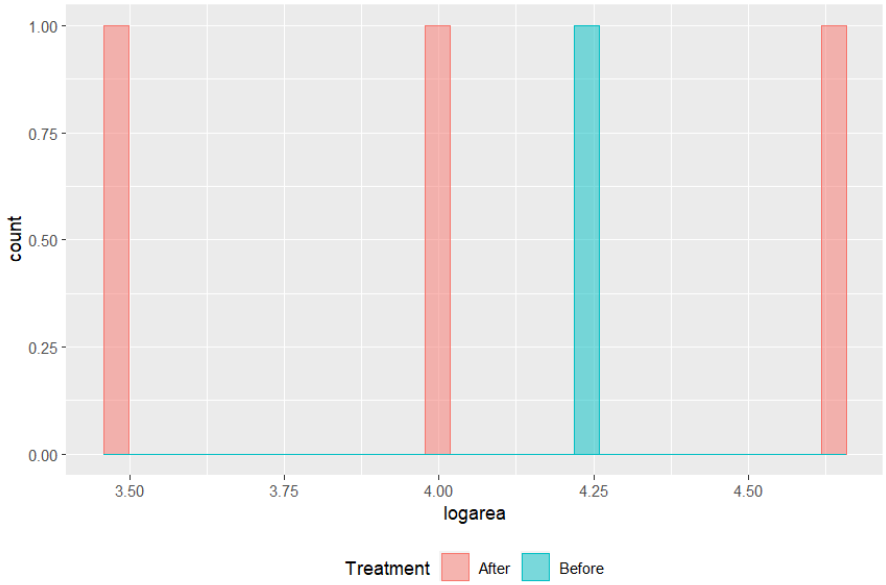

Figure 63. Size distribution of PS particles before and after Cellulose and Viscozyme treatment.

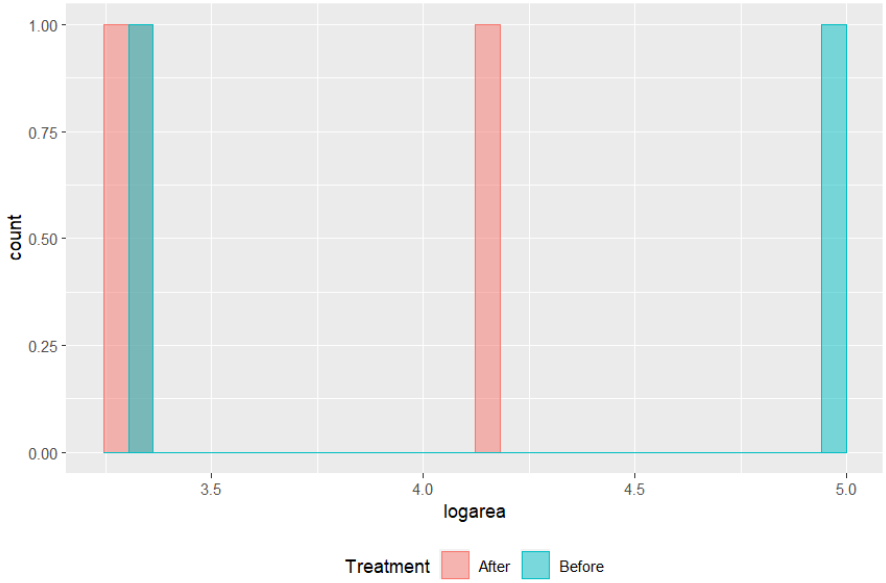

Figure 64. Size distribution of PS particles before and after Fenton oxidation.

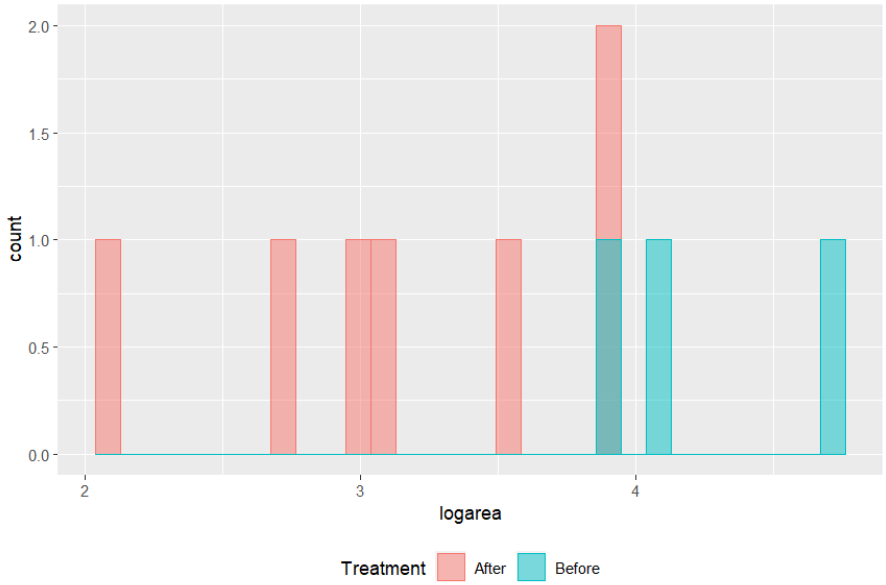

Figure 65. Size distribution of PS particles before and after Density separation.

The analysis of histograms presented provides insight into the changes in particle size distribution following the implementation of the different treatments in sample preparation. The observed histograms indicate the presence of smaller particles post-treatment in terms of the projected area, confirming the hypothesis that particle breakage or dispersion occurred during the treatment process. To gain insights into the central tendency of the data and analyze

changes in the distribution, median values of a projected area were calculated for the data presented in Figures 42 to 50. After the SDS treatment, the median for a projected area of PP particles significantly decreased. The median was 2571.3 μm^2 before the protocol step and decreased to 544.5 μm^2 after the treatment. Similar to this, following the protease treatment, the median size of PP particles dropped from 2934.3 μm^2 to 937.75 μm^2. In the case of cellulose and viscozyme treatment, the median decreased from 4325.8 μm^2 to 877.3 μm^2. The Fenton oxidation treatment also resulted in a reduction in median size, which fell from 1845.25 μm^2 to 847 μm^2. Regarding PE particles, the increase in particle count was observed only after the SDS treatment. The median for the projected area decreased from 14036 μm^2 to 5175 μm^2 after implementing this protocol step. For PS particles, the median size dropped after the protease treatment, from 33396 μm^2 to 287.4 μm^2. Similarly, the Fenton oxidation treatment resulted in a decrease in the median from 49065.5 μm^2 to 2117.5 μm^2. Lastly, the use of density separation reduced the median size from 12432.8 μm^2 to 1300.8 μm^2.

While particle breakage is a potential explanation for the changes in particle size, it could be that these alterations are a result of mechanical processes involved in the treatment procedure, such as sonication. These processes can induce fragmentation and dispersion of particles, leading to variations in their size distribution. To gain a comprehensive understanding of particle dynamics and the underlying factors influencing their size distribution changes, further investigations are needed. This may involve, for example, evaluating the influence of sonication parameters, and exploring potential mechanisms of particle aggregation and dispersion during the treatment process.

However, in Figure 45, which shows the size distribution of PP particles before and after the Fenton oxidation treatment, it is noticed that two particles exhibit a larger projected area after the treatment compared to their initial sizes. Similarly, Figure 48, illustrating the size distribution of PS particles before and after the cellulose and viscozyme treatment, shows the appearance of a particle with a larger projected area than any observed before the treatment. These anomalies can be attributed to the possibility of particle clustering or potential contamination with similar particles. For possible contamination with PE, PP, and PS particles, it is essential to point out the importance of using blank samples in order to determine whether the contamination with similar particles was caused by external conditions in the laboratory. It is possible to determine whether the presence of additional particles is solely due to contamination during the sample preparation process in the laboratory by analyzing blank samples alongside the prepared samples. This method would provide useful evidence for distinguishing genuine MP particles from those introduced during sample preparation and analysis, ensuring the accuracy and reliability of the results.

5. Conclusion

In conclusion, the investigation of the sample preparation protocol steps for both larger (500 µm - 3 mm) and smaller (2 µm - 200 µm) MP particles showed several findings. Regarding the effects of chemicals and techniques used in sample preparation on larger MPs, it was observed that these factors had minimal impact on the morphological and chemical properties of the particles. No significant changes in color, shape, or chemical composition were detected, except for potential effects on the shape of thin PET particles. Moreover, the most evident changes in particle spectra were observed after the SDS protocol step in sample preparation. These changes were primarily attributed to chemical residues remaining on the particles, highlighting the importance of thorough filtration with an abundant amount of water or even the use of ethanol. By implementing these measures, the accuracy of the subsequent analysis can be improved. All in all, the findings provide strong support for the ability of the implemented protocol to maintain the properties of the MP particles. By demonstrating that the sample preparation has minimal impact on the properties of the particles, the validity and integrity of the analysis are preserved.

Regarding smaller MP particles, it is concluded that filtering the entire sample onto the silicone membrane as a substrate for analysis, even in the absence of a matrix, did not give satisfactory results. Despite the "clean" nature of the sample, consisting of standard MP particles mixed in ethanol, the recovery rates for all protocol steps were not optimal. The presence of chemical residues and contamination disrupted the µFT-IR analysis. Thus, it is necessary to incorporate an evaporation step in the procedure and analyze only a representative portion of the sample, which can be upscaled. Moreover, the additional filtration can help in removing chemical residues. On the other side, it is noteworthy that some treatments resulted in a recovery rate exceeding 100% for PE, PP, and PS particles. Additionally, the size distribution analysis revealed a reduction in particle size after these treatments, indicating possible breakage or dispersion of particles during the protocol steps or potential contamination with similar particles. The appearance of possible contamination with the same particles highlights the importance of employing blank samples for the purpose of comparing and verifying the obtained results.

In summary, this study not only provided insights into sample preparation for MP analysis, but also opened the way for future studies to strengthen the standard methods in protocol and advance knowledge in this important field.

6. References

Eriksen, M., Lebreton, L. C., Carson, H. S., Thiel, M., Moore, C. J., Borerro, J. C. Galgani, F.,Ryan, P.G., Reisser, J. (2014). Plastic pollution in the world's oceans: more than 5 trillion plastic pieces weighing over 250,000 tons afloat at sea. PloS one, 9(12), e111913. DOI: https://doi.org/10.1371/journal.pone.0111913

Jambeck, J.R., Geyer, R., Wilcox, C., Siegler, T.R., Perryman, M., Andrady, A., Narayan, R., Law, K.L. (2018). Plastic waste inputs from land into the ocean. Science, 347(6223), 768-771. DOI: https://doi.org/10.1126/science.1260352

Lusher, A. L., McHugh, M., & Thompson, R. C. (2013). Occurrence of microplastics in the gastrointestinal tract of pelagic and demersal fish from the English Channel. Marine pollution bulletin, 67(1-2), 94-99. DOI: https://doi.org/10.1016/j.marpolbul.2012.11.028

Galloway, T.S., Cole, M., Lewis, C. (2017). Interactions of microplastic debris throughout the marine ecosystem. Nature Ecology & Evolution, 1(5), 0116. DOI: https://doi.org/10.1038/s41559-017-0116

Li, J., Liu, H., & Chen, J. P. (2018). Microplastics in freshwater systems: A review on occurrence, environmental effects, and methods for microplastics detection. Water Research, 137, 362-374. DOI: https://doi.org/10.1016/j.watres.2017.12.056

Rios, L.M., Moore, C., Jones, P.R. (2007). Persistent organic pollutants carried by synthetic polymers in the ocean environment. Marine Pollution Bulletin, 54(8), 1230-1237. DOI: https://doi.org/10.1016/j.marpolbul.2007.03.022

Wagner, M., Oehlmann, J. (2009). Endocrine disruptors in bottled mineral water: Total estrogenic burden and migration from plastic bottles. Environmental Science and Pollution Research, 16, 278–286 DOI: https://doi.org/10.1007/s11356-009-0107-7

Smith, M., Love, D.C., Rochman, C.M. and Nigam, R. (2018). Microplastics in Seafood and the Implications for Human Health. Current Environmental Health Reports, 5(3), pp.375-386. DOI: https://doi.org/10.1007/s11356-009-0107-7

GESAMP (2015). “Sources, fate and effects of microplastics in the marine environment: a global assessment” (Kershaw, P. J., ed.). (IMO/FAO/UNESCO IOC/UNIDO/WMO/IAEA/UN/UNEP/UNDP Joint Group of Experts on the Scientific Aspects of Marine Environmental Protection). Rep. Stud. GESAMP No. 90, 96 p.

Rasmussen, L. A., Iordachescu, L., Tumlin, S., & Vollertsen, J. (2021). A complete mass balance for plastics in a wastewater treatment plant-Macroplastics contributes more than microplastics. Environmental Pollution, 201, 117307. DOI: https://doi.org/10.1016/j.watres.2021.117307

Kirstein, I.V., Hensel, F., Gomiero, A., Iordachescu, L., Vianello, A., Wittgren, H.B., & Vollertsen, J. (2019). Drinking plastics? – Quantification and qualification of microplastics in drinking water distribution systems by µFTIR and Py-GCMS. Water Research, 188, 116519. DOI: https://doi.org/10.1016/j.watres.2020.116519

Yang, J., Monnot, M., Sun, Y., Asia, L., Wong-Wah-Chung, P., Doumenq, P., & Moulin, P. (2023). Microplastics in different water samples (seawater, freshwater, and wastewater): Methodology approach for characterization using micro-FTIR spectroscopy. Water Research, 232, 119711. DOI: https://doi.org/10.1016/j.watres.2023.119711

Hansen, J., Hildebrandt, L., Zimmermann, T., El Gareb, F., Fischer, E. K., & Pröfrock, D. (2023). Quantification and characterization of microplastics in surface water samples from the Northeast Atlantic Ocean using laser direct infrared imaging. Marine Pollution Bulletin, 190, 114880. DOI: https://doi.org/10.1016/j.marpolbul.2023.114880

Löder, M. G. J., Imhof, H. K., Ladehoff, M., Löschel, L. A., Lorenz, C., Mintenig, S., Piehl, S., Primpke, S., Schrank, I., Laforsch, C., & Gerdts, G. (2017). Enzymatic purification of microplastics in environmental samples. Environmental science & technology, 51(24), 14283-14292. DOI: https://doi.org/10.1021/acs.est.7b03055

Primpke, S., Christiansen, S. H., Cowger, W., De Frond, H., Deshpande, A., Fischer, M., Holland, E. B., Meyns, M., O'Donnell, B. A., Ossmann, B. E., Pittroff, M., Sarau, G., Scholz-Bottcher, B. M., & Wiggin, K. J. (2020). Critical Assessment of Analytical Methods for the Harmonized and Cost-Efficient Analysis of Microplastics. Appl Spectrosc., 74(9), 1012-1047. DOI: https://doi.org/10.1177/0003702820921465

PlasticsEurope. (n.d.). What are plastics? Retrieved from https://www.plasticseurope.org/en/about-plastics/what-are-plastics

Andrady, A. L. (2017). The plastic in microplastics: A review. Marine pollution bulletin, 119(1), 12-22. DOI: https://doi.org/10.1016/j.marpolbul.2017.01.082

Hartmann, N.B., Hüffer, T., Thompson, R.C., Hassellöv, M., Verschoor, A., Daugaard, A.E., Rist, S., Karlsson, T., Brennholt, N., Cole, M., Herrling, M.P., Hess, M.C., Ivleva, N.P., Lusher, A.L., Wagner, M. (2019). Microplastics in the Environment: Challenges in Analytical Chemistry

and Ecotoxicology. Environ. Sci. Technol., 53(3), 1039-1047. DOI: https://doi.org/10.1021/acs.est.8b05297

Van Cauwenberghe, L., Devriese, L., Galgani, F., & Robbens, J. (2015). Microplastics in sediments: A review of techniques, occurrence, and effects. Marine Environmental Research, 111, 5-17. DOI: https://doi.org/10.1016/j.marenvres.2015.06.007

Cole, M., Lindeque, P., Halsband, C., & Galloway, T. S. (2011). Microplastics as contaminants in the marine environment: A review. Marine Pollution Bulletin, 62(12), 2588-2597. DOI: https://doi.org/10.1016/j.marpolbul.2011.09.025

Corcoran, P.L. (2022). Degradation of Microplastics in the Environment. In: Rocha-Santos, T., Costa, M.F., Mouneyrac, C. (eds) Handbook of Microplastics in the Environment. Springer, Cham. DOI: https://doi.org/10.1007/978-3-030-39041-9_10

Kalogerakis, N., Karkanorachaki, K., Kalogerakis, G. C., Triantafyllidi, E. I., Gotsis, A. D., Partsinevelos, P., & Fava, F. (2017). Microplastics Generation: Onset of Fragmentation of Polyethylene Films in Marine Environment Mesocosms. Frontiers in Marine Science, 4, 84. DOI: https://doi.org/10.3389/fmars.2017.00084

Enfrin, M., Lee, J., Gibert, Y., Basheer, F., Kong, L., & Dumée, L. F. (2020). Release of hazardous nanoplastic contaminants due to microplastics fragmentation under shear stress forces. Journal of Hazardous Materials, 384, 121393. DOI: https://doi.org/10.1016/j.jhazmat.2019.121393

Guo, X., & Wang, J. (2019). The chemical behaviors of microplastics in marine environment: A review. Marine Pollution Bulletin, 142, 1-14. DOI: https://doi.org/10.1016/j.marpolbul.2019.03.019

Andrady, A. L. (2011). Microplastics in the marine environment. Marine Pollution Bulletin, 62(8), 1596-1605. DOI: https://doi.org/10.1016/j.marpolbul.2011.05.030

Dey, T.K., Uddin, M.E. & Jamal, M. (2021). Detection and removal of microplastics in wastewater: evolution and impact. Environ Sci Pollut Res 28, 16925–16947. DOI: https://doi.org/10.1007/s11356-021-12943-5

Khan, Shahid & Khan, Sher & Khan, Latif & Farooq, Aliya & Akhtar, Kalsoom & Asiri, Abdullah M. (2018). Fourier Transform Infrared Spectroscopy: Fundamentals and Application in Functional Groups and Nanomaterials Characterization. DOI: https://doi.org/10.1007/978-3-319-92955-2_9

Jiménez-Skrzypek, G., Ortega-Zamora, C., González-Sálamo, J., Hernández-Sánchez, C., & Hernández-Borges, J. (2021). The current role of chromatography in microplastic research: Plastics chemical characterization and sorption of contaminants. Journal of Chromatography Open, 1, 100001. DOI: https://doi.org/10.1016/j.jcoa.2021.100001

Ainali, N.M., Kalaronis, D., Kontogiannis, A., Evgenidou, E., Kyzas, G.Z., Yang, X., Bikiaris, D.N., Lambropoulou, D.A. (2021). Microplastics in the environment: Sampling, pretreatment, analysis and occurrence based on current and newly-exploited chromatographic approaches. Science of The Total Environment, 794, 148725. DOI: https://doi.org/10.1016/j.scitotenv.2021.148725

Kye, H., Kim, J., Ju, S., Lee, J., Lim, C., & Yoon, Y. (2023). Microplastics in water systems: A review of their impacts on the environment and their potential hazards. Heliyon, 9(3), e14359. DOI: https://doi.org/10.1016/j.heliyon.2023.e14359

Simon-Sánchez, L., Grelaud, M., Franci, M., & Ziveri, P. (2022). Are research methods shaping our understanding of microplastic pollution? A literature review on the seawater and sediment bodies of the Mediterranean Sea. Environmental Pollution, 292(Part B), 118275. DOI: https://doi.org/10.1016/j.envpol.2021.118275

Lee, H., Kim, S., Sin, A., Kim, G., Khan, S., Nadagouda, M.N., Sahle-Demessie, E., & Han, C. (2023). Pretreatment methods for monitoring microplastics in soil and freshwater sediment samples: A comprehensive review. Science of The Total Environment, 871, 161718. DOI: https://doi.org/10.1016/j.scitotenv.2023.161718

Gatidou, G., Arvaniti, O. S., & Stasinakis, A. S. (2019). Review on the occurrence and fate of microplastics in Sewage Treatment Plants. Journal of Hazardous Materials, 367, 504-512. DOI: https://doi.org/10.1016/j.jhazmat.2018.12.081

Nabi, I., Bacha, A.-U.-R., & Zhang, L. (2022). A review on microplastics separation techniques from environmental media. Journal of Cleaner Production, 337, 130458. DOI: https://doi.org/10.1016/j.jclepro.2022.130458

Molazadeh, M., Liu, F., Simon-Sánchez, L., & Vollersten, J. (2023). Buoyant microplastics in freshwater sediments – How do they get there? Science of The Total Environment, 860, 160489. DOI: https://doi.org/10.1016/j.scitotenv.2022.160489

Lenz, M., Brennecke, D., Haeckel, M., Knickmeier, K., & Kossel, E. (2023). Spatio-temporal variability in the abundance and composition of beach litter and microplastics along the Baltic Sea coast of Schleswig-Holstein, Germany. Marine Pollution Bulletin, 190, 114830. DOI: https://doi.org/10.1016/j.marpolbul.2023.114830

Carr, S.A., Liu, J., Tesoro, A.G., (2016). Transport and fate of microplastic particles in wastewater treatment plants. Water Res. 91, 174-182. DOI: https://doi.org/10.1016/j.watres.2016.01.002

Lavoy, M., & Crossman, J. (2021). A novel method for organic matter removal from samples containing microplastics. Environmental Pollution, 286, 117357. DOI: https://doi.org/10.1016/j.envpol.2021.117357

Carey, P. R. (1999). Raman Spectroscopy, the Sleeping Giant in Structural Biology, Awakes. Science, 274(5292), 26625-26628. DOI: https://doi.org/10.1074/jbc.274.38.26625

Baker, M.J., et al. (2014). Using Fourier transform IR spectroscopy to analyze biological materials. Nature Protocols, 9(8), 1771-1791. DOI: https://doi.org/10.1038/nprot.2014.110

Harvey, D.T. (2022) Instrumental Analysis. LibreTexts. https://chem.libretexts.org/Bookshelves/Analytical_Chemistry/Instrumental_Analysis_(LibreTexts)

Bumbrah, G. S., & Sharma, R. M. (2016). Raman spectroscopy – Basic principle, instrumentation and selected applications for the characterization of drugs of abuse. Egyptian Journal of Forensic Sciences, 6(3), 209-215. DOI: https://doi.org/10.1016/j.ejfs.2015.06.001

Anger, P. M., von der Esch, E., Baumann, T., Elsner, M., Niessner, R., & Ivleva, N. P. (2018). Raman microspectroscopy as a tool for microplastic particle analysis. TrAC Trends in Analytical Chemistry, 109, 214-226. DOI: https://doi.org/10.1016/j.trac.2018.10.010

Primpke, S., Cross, R.K., Mannigel, E., et al. (2020). Toward the Systematic Identification of Microplastics in the Environment: Evaluation of a New Independent Software Tool (siMPle) for Spectroscopic Analysis. Applied Spectroscopy, 74(9), 1127-1138. DOI: https://doi.org/10.1177/0003702820917760

Morgado, V., Gomes, L., Bettencourt da Silva, R. J. N., & Palma, C. (2021). Validated spreadsheet for the identification of PE, PET, PP and PS microplastics by micro-ATR-FTIR spectra with known uncertainty. Talanta, 234, 122624. DOI: https://doi.org/10.1016/j.talanta.2021.122624

Rist, S., Vianello, A., Winding, M. H. S., Nielsen, T. G., Almeda, R., Rodríguez Torres, R., & Vollertsen, J. (2020). Quantification of plankton-sized microplastics in a productive coastal Arctic marine ecosystem. Environmental Pollution, 266(Part 1), 115248. DOI: https://doi.org/10.1016/j.envpol.2020.115248